Monthly Notices of the ROYAL ASTRONOMICAL SOCIETY

MNRAS **538,** 518–536 (2025) https://doi.org/10.1093/mnras/staf269
Advance Access publication 2025 February 20

Signatures of black hole seeding in the local Universe: predictions from the BRAHMA cosmological simulations

Aklant K. Bhowmick [1]★ Laura Blecha,[2] Paul Torrey [1] Rachel S. Somerville [3] Luke Zoltan Kelley [4] Rainer Weinberger [5] Mark Vogelsberger [6] Lars Hernquist,[7] Priyamvada Natarajan [8,9,10] Jonathan Kho[1] and Tiziana Di Matteo [11]

[1]*Department of Astronomy, University of Virginia, Charlottesville, VA 22904, USA*
[2]*Department of Physics, University of Florida, Gainesville, FL 32611, USA*
[3]*Center for Computational Astrophysics, Flatiron institute, New York, NY 10010, USA*
[4]*Department of Astronomy, University of California at Berkeley, Berkeley, CA 94720, USA*
[5]*Leibniz Institute for Astrophysics Potsdam (AIP), An der Sternwarte 16, D-14482 Potsdam, Germany*
[6]*Department of Physics, Kavli Institute for Astrophysics and Space Research, Massachusetts Institute of Technology, Cambridge, MA 02139, USA*
[7]*Harvard-Smithsonian Center for Astrophysics, 60 Garden Street, Cambridge, MA 02138, USA*
[8]*Department of Physics, Yale University, New Haven, CT 06520, USA*
[9]*Department of Astronomy, Yale University, 266 Whitney Avenue, New Haven, CT 06511, USA*
[10]*Black Hole Initiative, Harvard University, 20 Garden Street, Cambridge, MA 02138, USA*
[11]*McWilliams Center for Cosmology, Carnegie Mellon University, Pittsburgh, PA 15213, USA*

Accepted 2025 February 11. Received 2025 January 17; in original form 2024 November 27

ABSTRACT

The origin of the 'seeds' of supermassive black holes (BHs) continues to be a puzzle, as it is currently unclear if the imprints of early seed formation could survive to today. We examine the signatures of seeding in the local Universe using five $[18\ \mathrm{Mpc}]^3$ BRAHMA simulation boxes run to $z = 0$. They initialize $1.5 \times 10^5\ \mathrm{M}_\odot$ BHs using different seeding models. The first four boxes initialize BHs as heavy seeds using criteria that depend on dense and metal-poor gas, Lyman–Werner radiation, gas spin, and environmental richness. The fifth box initializes BHs as descendants of lower mass seeds ($\sim 10^3\ \mathrm{M}_\odot$) using a new stochastic seed model built in our previous work. In our simulations, we find that the abundances and properties of $\sim 10^5 - 10^6\ \mathrm{M}_\odot$ local BHs hosted in $M_* \lesssim 10^9\ \mathrm{M}_\odot$ dwarf galaxies, are sensitive to the assumed seeding criteria. This is for two reasons: (1) there is a substantial population of local $\sim 10^5\ \mathrm{M}_\odot$ BHs that are ungrown relics of early seeds from $z \sim 5 - 10$; (2) BH growth up to $\sim 10^6\ \mathrm{M}_\odot$ is dominated by mergers in our simulations all the way down to $z \sim 0$. As the contribution from gas accretion increases, the signatures of seeding start to weaken in more massive $\gtrsim 10^6\ \mathrm{M}_\odot$ BHs, and they are erased for $\gtrsim 10^7\ \mathrm{M}_\odot$ BHs. The different seed models explored here predict abundances of local $\sim 10^6\ \mathrm{M}_\odot$ BHs ranging from $\sim 0.01 - 0.05\ \mathrm{Mpc}^{-3}$ with occupation fractions of $\sim 20 - 100$ per cent for $M_* \sim 10^9\ \mathrm{M}_\odot$ galaxies. These results highlight the potential for placing constraints on seeding models using local $\sim 10^5 - 10^6\ \mathrm{M}_\odot$ BHs hosted in dwarf galaxies. Since merger dynamics and accretion physics impact the persistence of seeding signatures, and both high and low mass seed models can produce similar local BH populations, disentangling their roles will require combining high and low redshift constraints.

Key words: methods: numerical – galaxies: evolution – galaxies: formation – quasars: supermassive black holes.

1 INTRODUCTION

The origin of supermassive black holes (SMBHs with masses $\gtrsim 10^6\ \mathrm{M}_\odot$) continues to be a key open question in our current understanding of galaxy formation. There are several promising seeding scenarios to account for them that span a wide range of initial seed masses. At the lowest mass end, the remnants of the first-generation Population III stars, often referred to as 'light seeds' or 'Pop III seeds' (Fryer, Woosley & Heger 2001; Madau & Rees 2001; Xu, Wise & Norman 2013; Smith et al. 2018) are viable candidates with typical masses of $\sim 100\ \mathrm{M}_\odot$. Runaway collisions of stars or black holes (BHs) in dense nuclear star clusters (NSCs), or the amplification of light seeds in the NSCs can form seeds as massive as $\sim 10^3 - 10^4\ \mathrm{M}_\odot$ (Davies, Miller & Bellovary 2011; Lupi et al. 2014; Kroupa et al. 2020; Das et al. 2021a, b; Natarajan 2021), referred to as 'NSC' seeds. More massive seeds can form under special conditions when the collapsing clouds of gas can circumvent the standard stellar evolution phases and directly collapse to form BHs in the very early Universe. The resulting seeds are referred to as direct collapse black holes or 'DCBH' seeds. They are typically considered to range between $\sim 10^4$ and $10^5\ \mathrm{M}_\odot$ (Bromm & Loeb 2003; Begelman, Volonteri & Rees 2006; Lodato & Natarajan 2006, 2007; Luo et al. 2018; Wise et al. 2019; Luo et al. 2020; Begelman &

★ E-mail: aklant.app@gmail.com

Silk 2023) but could form later on at $z \sim 6$ and proposed to be as massive as $\sim 10^8$ M$_\odot$ (Mayer et al. 2024).

A common feature amongst Pop III, NSC, and DCBH seeds is that the vast majority of them are expected to form within dense and low metallicity gas in the early Universe. At later times, seed formation is expected to slow down due to increased metal enrichment. Therefore, we expect the signatures of seeding to be most strongly retained within the early BH populations prior to efficient metal mixing. The first BH populations discovered at high z ($z \gtrsim 6$) prior to the ongoing *JWST*, were luminous quasars (bolometric luminosities $\gtrsim 10^{46}$erg s^{-1}) powered by BHs with masses ranging from $\sim 10^9$ to 10^{10} M$_\odot$ (Fan et al. 2001; Willott et al. 2010; Mortlock et al. 2011; Venemans et al. 2015; Bañados et al. 2016; Jiang et al. 2016; Reed et al. 2017; Bañados et al. 2018; Matsuoka et al. 2018, 2019; Wang et al. 2018, 2021; Yang et al. 2019). Explaining the assembly of these BHs within a billion years after the Big Bang continues to be challenging for BH seeding and growth models, likely requiring periods of super-Eddington growth.

The advent of *JWST* has further pushed the observational frontier, permitting detection of higher redshift active galactic nuclei (AGNs) populations at lower luminosities by detecting a large population of fainter broad-line (BL) AGN candidates at $z \sim 4-11$ (Greene et al. 2024; Harikane et al. 2023; Kocevski et al. 2023; Larson et al. 2023; Maiolino et al. 2024; Onoue et al. 2023; Akins et al. 2024; Andika et al. 2024; Kocevski et al. 2024). Remarkably, reported BH mass measurements ($\sim 10^6 - 10^8$ M$_\odot$) for several of the spectroscopically confirmed AGNs appear to be $\sim 10-100$ times more massive for their host galaxy stellar masses, compared to expectations from local galaxy scaling relations (Kokorev et al. 2023, 2024; Bogdán et al. 2024; Durodola, Pacucci & Hickox 2024; Kocevski et al. 2024; Natarajan et al. 2024). More recently, similarly overmassive BHs have also been observed at cosmic noon (Mezcua et al. 2024). While current BH mass and host galaxy stellar mass measurements do have substantial uncertainties (~ 1 dex), these overmassive BHs can be used to place further constraints on BH seeding and growth. Such exceptionally high $M_{\rm bh}/M_*$ ratios were predicted as a signature of heavy seeds (Agarwal et al. 2013; Natarajan et al. 2017, 2024), or efficient early growth of lower mass seeds via super-Eddington accretion (Trinca et al. 2024) or BH–BH mergers (Bhowmick et al. 2024b).

By the time we get to the local Universe, the signatures of seeding are expected to be washed out by the subsequent complex mass assembly history of BHs. However, if a small fraction of seeds do form at late times as noted by Natarajan (2021), or if there are seeds that formed earlier but did not undergo significant growth, these populations could retain some information about their initial seeding conditions. Moreover, since the initial seed populations are expected to lie at the lowest mass end of the BH mass functions and the faintest end of the AGN luminosity functions, they would be much more readily detectable (albeit still challenging to detect) in the local Universe compared to higher redshifts. Detection of intermediate mass black holes or IMBHs ($M_{\rm bh} \sim 10^3 - 10^5$ M$_\odot$) in local dwarf galaxies (stellar masses $M_* \lesssim 10^9$ M$_\odot$) is considered to be particularly promising for learning about BH seeds (see review by Reines 2022). Over the past two decades, numerous $M_{\rm bh} \sim 10^5 - 10^6$ M$_\odot$ IMBH candidates have been detected in local dwarf galaxies (Filippenko & Ho 2003; Barth et al. 2004; Greene & Ho 2004, 2007; Dong et al. 2012; Reines, Greene & Geha 2013; Mezcua et al. 2018; Schutte, Reines & Greene 2019; Molina et al. 2021; Angus et al. 2022; Ward et al. 2022; Yang et al. 2022; Häberle et al. 2024; Lin et al. 2024; Zuo et al. 2024), with the lowest mass detected IMBH being $\sim 50\,000$ M$_\odot$ (Baldassare et al. 2015). These developments have made it possible to probe the BH–galaxy scaling relations (Schutte et al. 2019; Baldassare et al. 2020; King & Nealon 2021; Angus et al. 2022) and BH occupation fractions (Greene 2012; Miller et al. 2015; Greene, Strader & Ho 2020) in the dwarf galaxy regime. Although uncertainties are substantial due to small sample sizes and challenges in BH mass measurements, they are a promising path for obtaining constraints on BH seeding and growth scenarios.

Several theoretical tools have been used to trace and make predictions for BH populations across cosmic time. Semi-analytic models (SAMs), due to their low computational expense, are able to robustly explore a wide range of BH seeding and growth scenarios and study their impact on observed properties (Barausse 2012; Ricarte & Natarajan 2018; Dayal et al. 2019; Sassano et al. 2021; Trinca et al. 2022; Chadayammuri et al. 2023; Spinoso et al. 2023; Trinca et al. 2023). However, SAMs do not track spatial information, like the detailed hydrodynamics of gas, which obviously plays a key role in BH formation and growth. This can only be done in full cosmological hydrodynamic simulations (Di Matteo et al. 2012; Vogelsberger et al. 2014b; Khandai et al. 2015; Schaye et al. 2015; Sijacki et al. 2015; Dubois et al. 2016; Volonteri et al. 2016; Kaviraj et al. 2017; Tremmel et al. 2017; Nelson et al. 2019a; Volonteri et al. 2020; Vogelsberger et al. 2020a). More recently, a class of hybrid SAMs have emerged that can extract the information about detailed gas properties from pre-existing cosmological simulations, and use them to build seed models (DeGraf & Sijacki 2020; Evans, Blecha & Bhowmick 2025). These hybrid SAMs retain the flexibility and efficiency of standard SAMs, while adding more physical realism in their seeding prescriptions. However, they are still not able to capture the impact of the BHs on the gas dynamics, since they only seed BHs in post-processing. Nevertheless, the limitations of SAM-based approaches are outshined by their computational efficiency. This has enabled them to systematically explore the impact of a wide range of seeding and growth prescriptions on BH populations all the way to the local universe (Ricarte & Natarajan 2018; Chadayammuri et al. 2023; Evans et al. 2025). All these studies show that BHs within local dwarf galaxies are strongly sensitive to the modelling of both BH seeding and BH growth.

Despite having self-consistent gas hydrodynamics, the modelling of BH seeding is extremely challenging in cosmological simulations. The substantial computational expense prohibits their ability to resolve the seeds and their formation processes in a cosmic volume. With a typical gas mass resolution of $\sim 10^5 - 10^6$ M$_\odot$, many galaxy formation simulations simply seed $\sim 10^5 - 10^6$ M$_\odot$ BHs based on a halo or stellar mass threshold (e.g. Di Matteo et al. 2012; Vogelsberger et al. 2014b; Khandai et al. 2015; Nelson et al. 2019a, b). Even though these simulations reproduce many of the observed local galaxy and BH properties (Habouzit et al. 2020, 2021), their implemented seeding prescriptions are too simplistic to provide any information about the origin of BH seeds. More recent simulations have adopted seeding models based on local gas properties that can better emulate the physical gas conditions for Pop III, NSC, or DCBH seeding, for e.g. seeding BHs within high density and low metallicity gas (Habouzit et al. 2016; Kaviraj et al. 2017; Tremmel et al. 2017; Jeon et al. 2025).

However, the formation conditions, initial masses, and formation rates of Pop III, NSC, and DCBH seeds are still very uncertain, which prevents us from ascertaining the best approaches to model them in cosmological simulations (as well as SAMs). For example, the initial mass function of Pop III stars is unknown, but that determines the formation rates and initial masses of Pop III seeds. For NSC seeds, there are uncertainties in the NSC occupation fractions within galaxies, as well as the final BH seed masses that can be grown in

an NSC via rapid amplification or runaway stellar and BH collisions (including the impact of gravitational recoil). DCBHs may require additional conditions beyond having a dense and pristine gas, such as strong Lyman Werner (LW) radiation (Shang, Bryan & Haiman 2010; Sugimura, Omukai & Inoue 2014; Wolcott-Green, Haiman & Bryan 2017), low gas spins (Lodato & Natarajan 2006), or dynamical heating induced by rapid halo growth (Wise et al. 2019; Regan et al. 2020b, c; Prole et al. 2024) (see also Natarajan 2021; Regan & Volonteri 2024). Lastly, there are also uncertainties in the modelling of BH accretion and dynamics in cosmological simulations (as well as SAMs) due to resolution limitations. This is expected to pose yet another challenge in constraining BH seeding and growth mechanisms from observations, due to potential degeneracies between the signatures of seeding, growth by accretion, and merger dynamics for BH populations. In the regime of local dwarf galaxies, Haidar et al. (2022) performed one of the largest studies to date comparing BH populations within five different cosmological simulations. They found that the different cosmological simulations result in widely different BH populations within dwarf galaxies. However, the reasons for these differences can be difficult to pin-point due to the variety of treatments deployed for initial BH seeding, accretion, and dynamics, as well as AGN and stellar feedback processes.

In light of these challenges, the BRAHMA simulation project (Bhowmick et al. 2024b, c) was started with the aim of performing a large systematic study to quantify the impact of seeding on BH populations across cosmic time. The BRAHMA simulations employ a set of novel seeding prescriptions that are based on gas properties within haloes, such as dense and metal-poor gas mass, LW radiation, gas spin, and halo environmental richness. The central idea is to explore different seeding model variations that cannot only encompass the different seeding scenarios (Pop III, NSC, and DCBH), but also encapsulate the different physics uncertainties within each model as noted above. All these seed models were extensively tested using high resolution zoom and constrained simulations (Bhowmick et al. 2021, 2022a, b). Furthermore, for large volume-low resolution simulations, we also built a novel stochastic seed model that can represent seeds that are $\sim 10-100$ times below the gas mass resolution limit (Bhowmick et al. 2024a). In our initial BRAHMA papers, we introduced a set of uniform simulation boxes (9, 18, and 36 Mpc box-size) and focused on making predictions for high-z BH populations for a set of low mass seed models emulating lower mass (Pop III and NSC) seeds (Bhowmick et al. 2024b) and heavy (DCBH) seeds (Bhowmick et al. 2024c).

In this work, we use a subset of boxes from Bhowmick et al. (2024b, c) to explore the impact of seeding on local BHs, particularly those living in dwarf galaxies ($M_* \lesssim 10^9$ M$_\odot$). We compare our predictions with existing observational constraints for BH populations in dwarf galaxies, as well as other theoretical predictions from SAMs and hydrodynamic simulations. One advantage we have compared to Haidar et al. (2022) is that apart from BH seeding, every other aspect of our galaxy formation model (including BH accretion and dynamics) is identical; this enables us to isolate the impact of seed formation in these populations. In Section 2, we summarize the key features of the BRAHMA simulations, along with the different seed models applied to the different boxes. Section 3 shows key predictions of a wide range of quantities including BH mass functions, AGN luminosity functions, $M_* - M_{\rm bh}$ relations, and the BH occupation fractions. In Section 4, we discuss the implications of our results on the viability of low mass (Pop III and NSC) seeds versus heavy (DCBH) seeds as possible origins of the observed local BH populations. Lastly, Section 5 summarizes the main conclusions of the paper.

2 THE BRAHMA SIMULATIONS

The BRAHMA simulation suite (Bhowmick et al. 2024a, c) was run using the AREPO gravity + magnetohydrodynamics (MHD) code (Springel 2010; Pakmor, Bauer & Springel 2011; Pakmor et al. 2016; Weinberger, Springel & Pakmor 2020). The *N*-body gravity solver uses the PM Tree (Barnes & Hut 1986) method whereas the MHD solver uses a dynamic unstructured grid generated via a Voronoi tessellation of the domain. The initial conditions were generated using MUSIC (Hahn & Abel 2011) and adopted a Planck Collaboration XIII (2016) cosmology i.e. $\Omega_\Lambda = 0.6911$, $\Omega_m = 0.3089$, $\Omega_b = 0.0486$, $H_0 = 67.74$ km sec^{-1}Mpc^{-1}, $\sigma_8 = 0.8159$, $n_s = 0.9667$. Haloes are identified using the friends of friends (FOF) algorithm (Davis et al. 1985) with a linking length of 0.2 times the mean particle separation. Subhaloes are computed at each simulation snapshot using the SUBFIND (Springel et al. 2001) algorithm.

The BRAHMA simulations were built to explicitly explore the impact of seeding models on BH populations across cosmic time. To that end, aside from seeding, every other aspect of the galaxy formation model has been kept the same as their predecessor Illustris-TNG simulations (Marinacci et al. 2018; Naiman et al. 2018; Nelson et al. 2018, 2019a; Springel et al. 2018; Pillepich et al. 2018b) which itself is based on the Illustris model (Vogelsberger et al. 2013; Torrey et al. 2014). Here we summarize the key features of the Illustris-TNG galaxy formation model.

Gas cooling and heating occurs in the presence of a uniform time-dependent UV background. Primordial gas cooling rates (from H, H^+, He, He^+, He^{++}) are calculated based on Katz, Weinberg & Hernquist (1996); metal cooling rates are interpolated from pre-calculated tables as in Smith, Sigurdsson & Abel (2008). Star formation occurs in gas cells with densities exceeding 0.15 cm^{-3} with an associated time-scale of 2.2 Gyr. These gas cells represent an unresolved multiphase interstellar medium described by an effective equation of state (Springel & Hernquist 2003; Vogelsberger et al. 2014a). The resulting star particles represent single stellar populations (SSPs) with an underlying initial mass function adopted from Chabrier (2003). The SSPs undergo stellar evolution based on Vogelsberger et al. (2013) with modifications for IllustrisTNG as described in Pillepich et al. (2018a). The resulting chemical enrichment of the SSPs follows the evolution of seven species of metals (C, N, O, Ne, Mg, Si, Fe) in addition to H and He. These metals pollute the surrounding gas via stellar and Type Ia/II supernova feedback, modelled as galactic scale winds (Pillepich et al. 2018b).

BHs can grow either via accretion or mergers. Gas accretion is modelled by the Eddington-limited Bondi–Hoyle formalism described as

$$\dot{M}_{\rm bh} = \min(\dot{M}_{\rm Bondi}, \dot{M}_{\rm Edd}) \tag{1}$$

$$\dot{M}_{\rm Bondi} = \frac{4\pi G^2 M_{\rm bh}^2 \rho}{c_s^3} \tag{2}$$

$$\dot{M}_{\rm Edd} = \frac{4\pi G M_{\rm bh} m_p}{\epsilon_r \sigma_T\, c}, \tag{3}$$

where G is the gravitational constant, ρ is the local gas density, $M_{\rm bh}$ is the BH mass, c_s is the local sound speed, m_p is the proton mass, and σ_T is the Thompson scattering cross-section. Accreting BHs radiate at bolometric luminosities given by

$$L_{\rm bol} = \epsilon_r \dot{M}_{\rm bh} c^2, \tag{4}$$

with an assumed radiative efficiency of $\epsilon_r = 0.2$. A portion of the radiated energy couples to the surrounding gas as AGN feedback, which is implemented as two distinct modes depending on the Eddington ratio η. For high Eddington ratios ($\eta > \eta_{\rm crit} \equiv$

min[0.002($M_{\rm BH}/10^8{\rm M}_\odot)^2$, 0.1]), 'thermal feedback' is implemented wherein a fraction of the radiated luminosity is deposited to the gas at a rate of $\epsilon_{f,\rm high}\epsilon_r\dot{M}_{\rm BH}c^2$ with $\epsilon_{f,\rm high}\epsilon_r = 0.02$ ($\epsilon_{f,\rm high}$ is the 'high accretion state' coupling efficiency). For low Eddington ratios ($\eta < \eta_{\rm crit}$), feedback is in the form of kinetic energy that is injected onto the gas at irregular time intervals along a randomly chosen direction. The rate of injection is given by $\epsilon_{f,\rm low}\dot{M}_{\rm BH}c^2$ with $\epsilon_{f,\rm low}$ being the 'low accretion state' coupling efficiency ($\epsilon_{f,\rm low} \lesssim 0.2$). Please see Weinberger et al. (2017) and Terrazas et al. (2020) for further details.

We note here that the Bondi prescription is rather simplistic, as it was originally derived for a spherically symmetric accretion flow wherein the gravitational force on the accreting gas is dominated by the BH. In reality, the gas can be self-gravitating (particularly cold dense gas) and have substantial angular momentum. Moreover, it has been recently shown that even in the case of spherically symmetric accretion, magnetic fields can suppress the accretion rates by factors of ~ 100 compared to the Bondi–Hoyle prediction (Cho et al. 2023). Nevertheless, our current BRAHMA boxes continue to use Bondi–Hoyle accretion because (1) it has been used in their predecessor IllustrisTNG simulations to successfully reproduce many of the observed galaxy and BH properties, and (2) we want to isolate the impact of seed models on our BH populations. In the near future, we shall be exploring seed models with alternate accretion prescriptions (Weinberger et al., in preparation; Burger et al., in preparation).

Finally, BH dynamics cannot be naturally resolved in our simulations, since the DM particle masses are ~ 10 times larger than the BH masses. To prevent artificially large kicks arising from DM particles, we 're-position' the BHs to the nearest potential minimum within their 'neighbourhood' (defined by $n^{\rm gas}_{\rm ngb} = 64$ nearest neighbouring gas cells). BHs are promptly merged when at least one of them is within the 'neighbour search radius' ($R_{\rm Hsml}$ comprising of $n^{\rm gas}_{\rm ngb}$ gas cells) of the other. We note that our repositioning scheme can potentially overestimate the contributions of both mergers and gas accretion to the overall BH growth. We will investigate the behaviour of our seed models under a subgrid dynamical friction (subgrid-DF) models in a follow-up paper.

2.1 BH seeding models and the resulting simulation suite

The key novel feature of BRAHMA is the numerical implementation of new physically motivated prescriptions for BH seeding. These prescriptions were originally developed and tested in our previous work using high resolution zoom simulations (Bhowmick et al. 2021, 2022a, 2024a), and subsequently implemented in the uniform suite of BRAHMA simulations (Bhowmick et al. 2024b, c). The existing BRAHMA suite consists of > 15 uniform boxes wherein we systematically explore a large ensemble of seed models that span a wide range of seeding environments as well as seed masses ranging from $\sim 10^3$ and 10^6 $\rm M_\odot$.

In this paper, we select a subset of [18 Mpc]^{3}BRAHMA boxes that were run to $z = 0$ using 512^3 dark matter (DM) particles and equal number of initial gas cells for analysis. The resulting DM mass resolution 1.5×10^6 $\rm M_\odot$ and the gas mass and stellar mass resolution is $\sim 10^5$ $\rm M_\odot$. The comoving gravitational softening length is 0.72 kpc for DM, stars, and BH particles. For the gas cells we use an adaptive softening scheme that depends on the cell radius, with a minimum softening of 0.72 kpc. These boxes seed BHs close to their gas mass resolution; i.e. 1.5×10^5 $\rm M_\odot$. Depending on our seed models, these initial BHs can be interpreted either as being directly formed as *heavy* seeds, or as *extrapolated descendants* of unresolved lower mass seeds (as explained below).

2.1.1 Heavy seed models

To model heavy seeds, we use distinct combinations of the following four seeding criteria that are motivated by presumed feasible environments for DCBH formation as first proposed by Lodato & Natarajan (2006):

(i) *Dense and metal-poor gas mass criterion:* When this criterion is applied, seeds are able to form only in haloes that exceed a critical gas mass threshold that is simultaneously dense enough to form stars ($\gtrsim 0.15$ cm^{-3}), and yet devoid of metals ($Z \lesssim 10^{-4}$ $Z_\odot$). There is no obvious choice for what the best value for this threshold is, and we have explored a range of possibilities from $\sim 5 - 150$ $M_{\rm seed}$ in Bhowmick et al. (2021) using zoom simulations run till $z = 7$. The variations these differing choices produce in the overall seed abundances and $z = 7$ BH masses are about a factor of ~ 10. In this work, we choose a lenient threshold of 5 $M_{\rm seed}$, such that we could thereafter combine additional seeding criteria (described below) and still form sufficient numbers of seeds within our simulation volume.

(ii) *LW flux criterion:* This criterion further requires the dense and metal-poor gas mass to be exposed to a minimum Lyman Werner (LW) flux of 10 J_{21}. In the absence of a full radiative transfer calculation, the local LW intensity was computed using an analytical formalism adopted from Dijkstra, Ferrara & Mesinger (2014). We include LW flux contributions from Pop III and Pop II star particles with ages < 5 Myr, defined based on metallicity ranges of $< 10^{-3}$ $Z_\odot$ and $10^{-3} - 10^{-1}$ $Z_\odot$, respectively. For readers interested in more detail about the LW flux calculation, please refer to section 2.1.2 of Bhowmick et al. (2022a).

Halo mass criterion: We only allow seeding in sufficiently resolved haloes (with > 32 DM particles). Therefore, the resolution limit of our simulations also implicitly imposes an additional halo mass threshold of 4.8×10^7 $\rm M_\odot$ for seeding. Note that this threshold is well within the atomic cooling limit that evolves from $\sim 10^7$ $\rm M_\odot$ to 10^8 $\rm M_\odot$ from $z \sim 20$ to 0. One could use higher resolution simulations to explore the formation of heavy seeds in even smaller haloes, but that would require additional physics that are not included in our simulations (for e.g. H_2 cooling). We shall explore this in future work.

(iii) *Gas-spin criterion:* This criterion restricts seeding to haloes with a gas spin that is below the Toomre instability threshold. The adoption of this criterion was based on Lodato & Natarajan (2006) and the detailed description is provided in Bhowmick et al. (2022a).

(iv) *Halo environment criterion:* This criterion allows seeding to only occur in haloes in rich environments; i.e. they have at least one neighbour of comparable or higher mass within a distance of five times the virial radius. This is intended to capture the impact of dynamical heating in rapidly growing haloes during major mergers, which has been shown to substantially alleviate the stringent requirement of strong LW fluxes for DCBH formation (Wise et al. 2019; Regan et al. 2020b).

We use the same four heavy seed model simulation boxes as Bhowmick et al. (2024c). The seed models in these boxes were constructed by incrementally stacking the above seeding criteria: The first box (SM5) only applies the *dense and metal-poor gas mass criterion* and the implicitly applied *halo mass criterion*. The second box (SM5_LW10) additionally applies the *LW flux criterion*. The third box (SM5_LW10_LOWSPIN) further adds the *gas-spin criterion*. The

fourth box (SM5_LW10_LOWSPIN_RICH) also includes the *halo environment criterion*. Since these models assume that the initial 1.5×10^5 $M_\odot$ BHs were directly formed as heavy seeds, we shall hereafter refer to them as *direct heavy seeds* or 'DHS'. We also note that these DHS models will produce much more numerous heavy seeds compared to canonical DCBH formation scenarios discussed in the literature that require extremely high critical LW fluxes ($\gtrsim 1000\ J_{21}$). Based on the results from our previous work (Bhowmick et al. 2022a), we expect an extremely small number of seeds (if any) to be produced in our boxes at such high critical LW fluxes. Therefore, we do not include these very restrictive DCBH formation scenarios in this paper, as we do not expect them to be the origins for the bulk of the locally observed SMBH populations.

2.1.2 Low-mass seed models

Low-mass seeds are generally challenging to model in cosmological simulations due to the difficulty in directly resolving them. To that end, in Bhowmick et al. (2024a), we developed a novel stochastic seed model that can faithfully capture the higher mass descendants of seeds that are $\sim 10-100$ times below the simulation mass resolution. Since the initial BHs in this case are descendants of the *actual* seeds, we refer to them as *extrapolated seed descendants* or ESDs. These models are directly calibrated using highest resolution simulations that explicitly resolve our target low-mass seeds. In this work, our target seed mass is 2.2×10^3 $M_\odot$. To ensure that our 1.5×10^5 $M_\odot$ ESDs faithfully represent descendants of $\sim 10^3$ $M_\odot$ seeds, the stochastic seed model uses the following three seeding criteria:

(i) *Stochastic galaxy mass criterion*: When this criterion is applied, ESDs are formed in galaxies[1] over a broad distribution of total masses (star+gas+DM) that evolves with redshift. This criterion is required because in Bhowmick et al. (2024a, b), descendants of 2.2×10^3 $M_\odot$ seeds were found to assemble in galaxies spanning a broad distribution of masses.

(ii) *Stochastic galaxy environment criterion*: This criterion preferentially forms ESDs in galaxies living in rich environments with a higher number of comparable or more massive neighbours. The need for this criterion arose because of the merger-dominated growth of 2.2×10^3 $M_\odot$ seeds at $z \gtrsim 3$ (as we found in Bhowmick et al. 2024a, b). More specifically, the mergers lead to preferentially higher BH growth in galaxies living in rich environments (at fixed galaxy mass) since they had a more extensive merger history.

(iii) *Unresolved minor mergers*: Since our simulations cannot capture BH growth due to mergers where the primary BH is resolvable but the secondary BH is not (i.e. the secondary BH mass is lower than the ESD mass), their contribution is explicitly added to the simulations.[2] More specifically, for every resolved merger event, we add an additional contribution equal to four times the ESD mass to account for mass growth due to unresolved minor mergers. This contribution was calibrated based on results from high resolution simulations of Bhowmick et al. (2024b) that explicitly resolve these minor mergers.

Key inputs for our stochastic seed model include the shape and the time-evolution of the galaxy mass distribution, seed probability as a function of galaxy neighbour counts, and the BH growth rate due to unresolved minor mergers. These inputs are provided by high resolution simulations[3] that explicitly resolve our target seed mass of 2.2×10^3 $M_\odot$. In other words, the stochastic seed model is designed to ensure that ESDs are placed in those environments wherein the high resolution simulations would naturally assemble descendant BHs comparable to the ESD mass. For full details of the modelling and calibration of the stochastic seed model, please refer to Bhowmick et al. (2024a). Our fifth and final simulation box used in this work applied this stochastic seed model and is labelled as 'ESD:STOCHASTIC'.

To summarize, our simulation suite comprises of five [18 Mpc]^3 boxes that initialize BHs at 1.5×10^5 $M_\odot$. The first four boxes apply the DHS seed models, namely SM5, SM5_LW10, SM5_LW10_LOWSPIN, and SM5_LW10_LOWSPIN_RICH, wherein the initial BHs can be interpreted as heavy seeds born out of direct collapse. In the fifth ESD:STOCHASTIC box, the initial BHs are interpreted as descendants of lower mass $\sim 10^3$ $M_\odot$ seeds. Note that for these relatively small boxes, the results may be impacted by missing large-scale modes as well as cosmic variance. However, as we shall see later, our predicted local BH mass functions are similar to those from the much larger IllustrisTNG simulations for $\gtrsim 10^7$ $M_\odot$ BHs. This indicates that at least for the quantities we are interested in, such as mass functions and occupation fractions of $\sim 10^5 - 10^8$ $M_\odot$ BHs, the results are not substantially impacted by our limited volume. Lastly, these small volumes are not able to probe the high mass end of the galaxy and BH populations. However, our key focus here is on the low mass end, particularly the local dwarf galaxies, which these simulations can effectively probe.

3 RESULTS

We examine a range of properties that describe the $z = 0$ BH populations with the goal of assessing how sensitive they are to the seed models. Fig. 1 shows a visualization of the spatial distributions of $z = 0$ BH populations throughout the simulation volumes, plotted on top of the 2D gas density and metallicity profiles. For the most lenient DHS model i.e. SM5, the most massive BHs are formed in the most overdense regions that are typically at the intersections of filaments. In addition, there is a more abundant population of lower mass BHs in less overdense regions, typically along the filaments. As we make the DHS models more restrictive, the lower mass BHs residing along the filaments are suppressed whereas the most massive BHs remain virtually unaffected. The ESD model contains substantially fewer numbers of BHs than the most lenient DHS model, but a larger number of BHs than the most restrictive DHS model. However, note that here we are only counting the number of $\gtrsim 10^5$ $M_\odot$ BHs whereas the ESD model is meant to represent a Universe that should also contain a much larger number of $\sim 10^3$ $M_\odot$ seeds that cannot be resolved in our boxes. Overall, the above results hint that the low mass end of the local BH population is indeed sensitive to the choice of our seed model, which we quantify in more detail in the following subsections.

[1]Note here that *galaxies* here are essentially identified as friends-of-friends groups, but they have 1/3 of the standard linking-length compared to haloes. We refer to these objects as 'best friends-of-friends' or bFOFs. We place ESDs in bFOFs instead of FOFs to accommodate the possibility of multiple seed descendants per halo.

[2]The simulations that use the stochastic seed model also do not explicitly resolve mergers wherein *both* primary and secondary BHs are below the ESD mass. However, their contributions are implicitly included in the creation of ESDs via the *stochastic galaxy mass and environment criterion*.

[3]These are 9 Mpc box simulations that resolve the gas down to $\sim 10^3$ $M_\odot$ resolution. They are referred to as BRAHMA-9-D3 simulations in Bhowmick et al. (2024b).

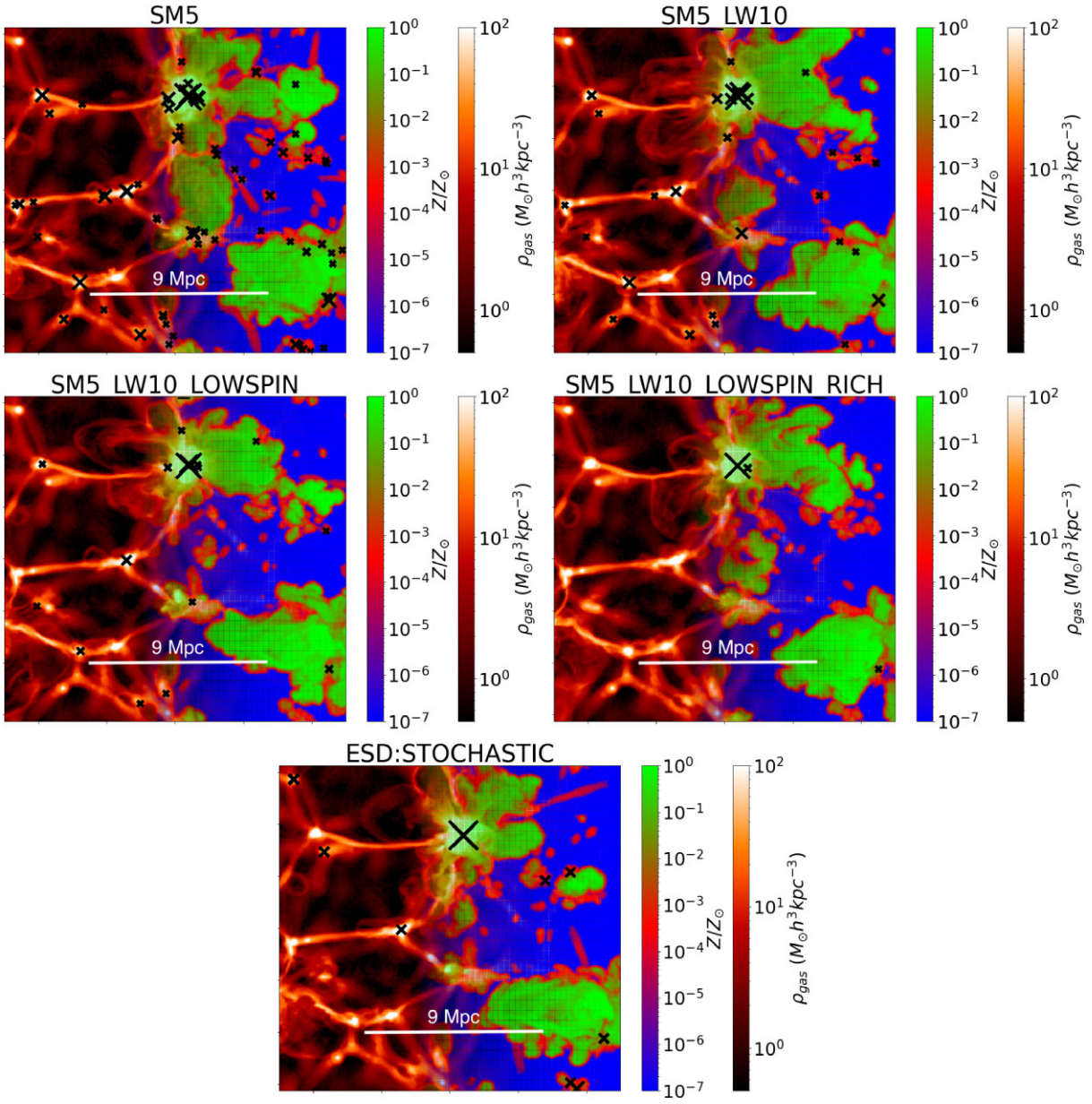

Figure 1. Visualizations of the $z = 0$ universe in our $[18\ \mathrm{Mpc}]^3$ simulation boxes that use the different seed models with an initial mass of $1.5 \times 10^5\ \mathrm{M}_\odot$. The left side of the boxes shows the gas density profiles and the right side shows the gas metallicity profiles at $z = 0$, averaged over a 200 kpc thick slice along the line-of-sight coordinate. The top four boxes (`SM5`, `SM5_LW10`, `SM5_LW10_LOWSPIN`, and `SM5_LW10_LOWSPIN_RICH`) show four models that assume the initial BHs are directly formed as heavy seeds (hereafter'direct heavy seeds' or 'DHS'). The lowermost box (`ESD:STOCHASTIC`) uses a stochastic seed model built in Bhowmick et al. (2024a) that assumes that the initial BHs are descendants of lower mass seeds (hereafter' extrapolated seed descendants' or 'ESDs'). BHs are represented by the black crosses with sizes commensurate to their masses. All the seed models produce the most massive BHs in the most overdense regions at the intersections of filaments. However, the more lenient seed models produce much larger numbers of lower mass BHs compared to the stricter seed models.

3.1 Seed formation history

While this paper focuses on $z = 0$, it is imperative to first look at the overall seed formation history in order to contextualize the results in the local Universe. Fig. 2 shows the rate at which new seeds are forming per unit redshift. For the four DHS models, the first episodes of seed formation occur around $z \sim 24$ as the first regions of dense (star forming) gas start to emerge. As the redshift decreases, seed formation continues to increase until it peaks at $z \sim 10$. After $z \sim 10$, this mode of seed formation slows down. In our previous works, we primarily talked about metal enrichment as the cause for the slow down and suppression of seed formation at late times. However, there is also some contribution from stellar feedback and cosmological expansion as they reduce the ability of haloes (of a fixed mass) to form dense and star forming gas at later times. In addition, the UV background (switched on at $z = 6$) is also expected to further suppress the formation of dense and star forming gas. With that being said, metal enrichment still remains the major impediment to seed formation at late times. However, even haloes that are undergoing metal enrichment, can (and do) form seeds. In fact, as demonstrated in our previous papers (Bhowmick et al. 2022a,

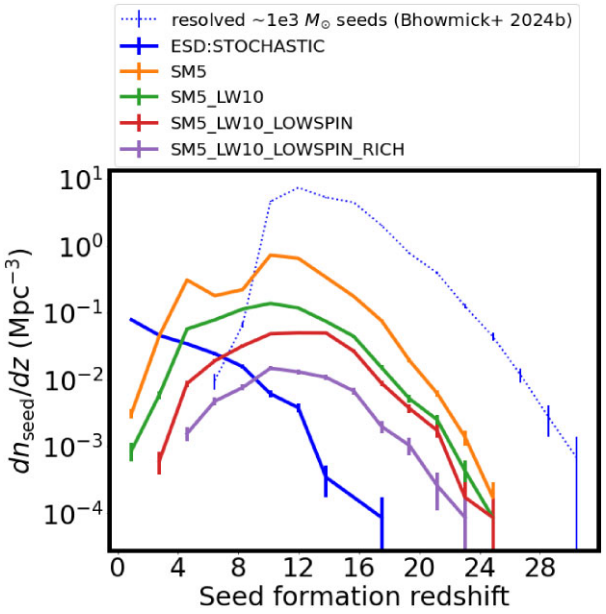

Figure 2. The number density of new seeds that form at various redshifts. Predictions for the four DHS models: `SM5`, `SM5_LW10`, `SM5_LW10_LOWSPIN`, and `SM5_LW10_LOWSPIN_RICH`, are shown as solid lines in orange, green, red, and purple, respectively. The blue solid line shows the ESD model (`ESD:STOCHASTIC`) that seeds 1.5×10^5 M$_\odot$ BHs as if they are descendants of unresolved lower mass $\sim 10^3$ M$_\odot$ seeds. The ESD model was calibrated from higher resolution simulations that explicitly resolve the $\sim 10^3$ M$_\odot$ seeds; the dotted line shows the number density and halo mass distributions of the actual $\sim 10^3$ M$_\odot$ seeds that were fully resolved in a [9 Mpc]^3 high resolution box from Bhowmick et al. (2024b). Therefore, the dotted and solid blue lines are meant to represent the same underlying physical seed model. The foregoing colour scheme for the different boxes is the same for all the figures hereafter. While DHSs emerge earlier than the ESDs, their formation is suppressed by metal-enrichment at $z \lesssim 10$. On the other hand, even though ESDs emerge later, they continue to form in higher numbers at decreasing redshifts, all the way to $z \sim 0$.

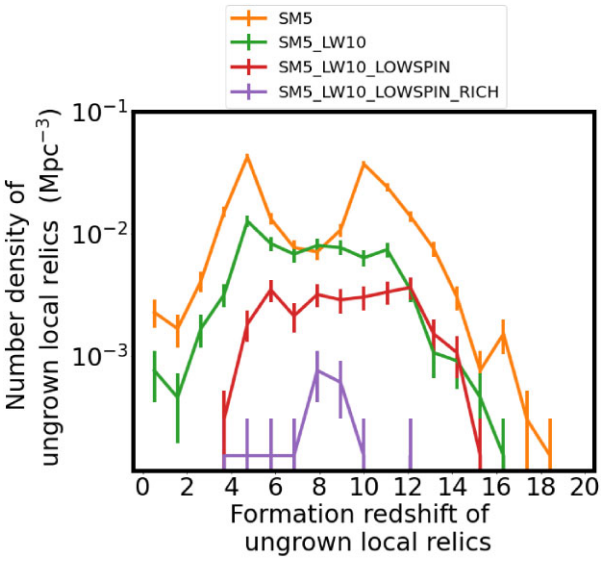

Figure 3. For our four DHS models, we show the distribution (number density per unit redshift bin) of the formation redshifts of seeds that did not undergo any significant growth via accretion or mergers all the way down to $z = 0$. Specifically, we select seeds that only grew by $\lesssim 10$ per cent of their initial mass. We find that in all four DHS models, most of these ungrown seeds were formed in the Universe between $z \sim 5 - 10$.

2024a, b), many of our seeds form in transient pockets of dense and metal-poor gas in partially metal-enriched haloes. Therefore, in the two most lenient DHS models (`SM5` and `SM5_LW10`), there is some amount of seed formation that continues to occur all the way to $z = 0$. For the two more restrictive DHS models, `SM5_LW10_LOWSPIN` and `SM5_LW10_LOWSPIN_RICH`, the last seeds form around $z \sim 3$ and $z \sim 5$, respectively; however, even for these models, some amount of seed formation could have happened at lower redshifts if our boxes were larger.

The seeds that form very close to $z \sim 0$ do not have enough time to grow into higher mass BHs. Therefore, these seeds will populate the lowest mass end of the local BH mass functions. However, the low mass end of the local BH mass functions will also be populated by seeds that form at higher redshifts but do not grow appreciably via either accretion or mergers by $z \sim 0$. In Fig. 3, we take the four DHS models and plot the distribution of formation redshifts for those seeds that undergo negligible growth ($\lesssim 10$ per cent of their initial seed mass) by $z \sim 0$. We can readily see that for all DHS models, the majority of the ungrown BHs are local relics of seeds that formed between $z \sim 5 - 10$. While these ungrown seeds do (unsurprisingly) form at lower redshifts compared to when most seeds form in general ($z \sim 12$), they still form at relatively high redshift compared to $z = 0$. We show in Sections 3.2 and 3.3 that these local relics of higher redshift seeds ($z \sim 5 - 10$) essentially dominate the lowest mass end of our simulated local BH populations, which therefore has a strong sensitivity to the BH seed models in their overall abundances.

Interestingly, for the `SM5` model, the distributions in Fig. 3 (orange lines) have two peaks at $z \sim 10$ and $z \sim 5$. While the peak at $z \sim 10$ coincides with the peak in the overall seed formation history shown in Fig. 2, the second peak at $z \sim 5$ is caused by a noticeable temporary phase of enhancement in the overall seed formation rates around $z \sim 5$ (orange lines in Fig. 2). This enhancement occurs due to a small uptick in the number of new star forming haloes at $z \sim 5$. Since there are several effects that impact the formation of dense star forming gas in haloes (e.g. mergers, stellar feedback, UV background etc.), it is not immediately obvious why such an uptick should occur at $z \sim 5$. However, we suspect that it is a numerical artefact arising from suddenly turning on the UV background at $z = 6$ as it leads to a artificially rapid decrease of the cold neutral gas density due to ionization, but soon followed by a rapid increase in the density due to recombination (Gabrielpillai et al., in preparation). We see hints of similar enhancements in seed formation at $z \sim 5$ even in the more restrictive DHS models, but they are much less pronounced compared to the `SM5` model. In future simulations, we plan to implement a more gradual evolution for the UV background. For this work, since this secondary peak at $z \sim 5$ is much smaller than the peak at $z \sim 10$, it is unlikely to have a strong impact on the main conclusions.

For the ESD model (blue line in Fig. 2), the (extrapolated) 1.5×10^5 M$_\odot$ seeds start to form at $z \sim 16$, which is significantly delayed compared to the DHS models. Recall again that the ESDs are meant to be descendants of unresolved lower mass $\sim 10^3$ M$_\odot$ seeds. The blue dotted line in Fig. 2 shows the seed formation history of the $\sim 10^3$ M$_\odot$ seeds from one of the high resolution boxes of Bhowmick et al. (2024b) where they were explicitly resolved (the ESD model was calibrated using this simulation). In this simulation, the 2.2×10^3 M$_\odot$ seeds were placed in haloes with sufficient dense and metal-poor gas mass ($> 10^4$ M$_\odot$) and total mass ($> 6 \times 10^6$ M$_\odot$). As we can see, the $\sim 10^3$ M$_\odot$ seeds form in much higher numbers (per unit volume) than any of the DHS models. Despite this, their higher mass $\sim 10^5$ M$_\odot$

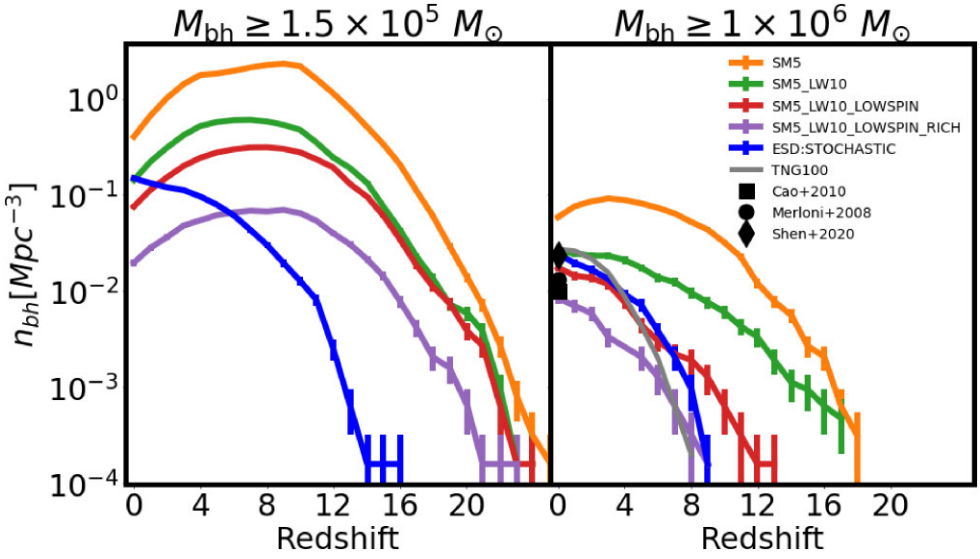

Figure 4. Comoving number density evolution of $\gtrsim 10^5$ and $\gtrsim 10^6$ $M_\odot$ BHs are shown in the left and right panels, respectively. Black data points show the local observational constraints from Merloni & Heinz (2008), Cao (2010) and Shen et al. (2020). The grey line shows the prediction from the TNG100 simulation. The $z = 0$ number densities exhibit significant seed model variations for both $\gtrsim 10^5$ and $\gtrsim 10^6$ $M_\odot$ BHs.

descendants start forming significantly later than the DHS models. In other words, it takes longer to grow $\sim 10^5$ $M_\odot$ BHs from lower mass seeds, compared to directly producing the $\sim 10^5$ $M_\odot$ BHs as heavy seeds using our DHS models. However, while seed-formation in our DHS models is slowed down by metal-enrichment at $z \lesssim 10$, the ESD model continues to produce an increasing number of $\sim 10^5$ $M_\odot$ ESDs down to much lower redshifts. To that end, the production of $\sim 10^5$ $M_\odot$ ESDs continues to increase all the way to $z = 0$, even though the formation of the $\sim 10^3$ $M_\odot$ seeds is strongly suppressed by metal enrichment at $z \lesssim 10$ (revisit dotted blue line in Fig. 2). This is because even if there are extremely small number of new $\sim 10^3$ $M_\odot$ seeds at $z \lesssim 10$, the existing seeds continue to merge with one another and form new $\sim 10^5$ $M_\odot$ ESDs all the way to $z = 0$.

3.2 BH number density evolution

Fig. 4 shows the number density[4] evolution of $\gtrsim 10^5$ $M_\odot$ and $\gtrsim 10^6$ $M_\odot$ BHs. Let us first focus on $\gtrsim 10^5$ $M_\odot$ BHs (left panel). As expected from the seed formation history, in the DHS models, the number density of $\gtrsim 10^5$ $M_\odot$ BHs steadily increases with time between $z \sim 24 - 10$. At $z \lesssim 10$ when new seed formation starts to drop, the number density steadily decreases from $z \sim 10 - 0$. This is because the existing seeds start to merge with one another. At $z = 0$, the number densities predicted by the DHS models vary from $0.02 - 0.4$ Mpc^{-3}. Recall from the previous section that these number densities are essentially dominated by the local ungrown relics of high-redshift ($z \sim 5 - 10$) seeds. The ESD seed model, because of its distinct seed formation history, also has a distinct number density evolution compared to the DHS models. While the number density decreases from $z \sim 12$ to $z \sim 0$ in the DHS models, it steadily increases from $z \sim 16$ to $z \sim 0$ in the ESD model. Consequently, despite having substantially smaller number densities compared to the DHS models at $z \gtrsim 7$, the ESD model catches up with the DHS models at $z = 0$. The ESD model predicts a $z = 0$ number density of ~ 0.1 Mpc^{-3} for $\gtrsim 10^5$ $M_\odot$ BHs, which is similar to the two intermediary DHS models (`SM5_LW10` and `SM5_LW10_LOWSPIN`). This is ~ 8 times larger than the most restrictive DHS model (`SM5_LW10_LOWSPIN_RICH`), while being ~ 2 times fewer than the most lenient DHS model (`SM5`). Overall, between the ESD model and the four DHS models, variations in the number densities of $\gtrsim 10^5$ $M_\odot$ BHs can be up to factors of ~ 20. This implies that future measurements of the number density of $\gtrsim 10^5$ $M_\odot$ BHs in the local Universe could provide strong constraints for seed models, so long as we are able to disentangle the impact of seeding from that of other BH physics such as dynamics and accretion. Now we focus on the number density of $\gtrsim 10^6$ $M_\odot$ BHs (right panel of Fig. 4). At $z = 5$, the seed model variations in the number density span more than two orders of magnitude from a few times $\sim 10^{-4}$ to $\sim 6 \times 10^{-2}$ Mpc^{-3}. As we get to lower redshifts, the seed model variations start to become smaller. By $z = 0$, the number density of $\gtrsim 10^6$ $M_\odot$ BHs varies by a factor of ~ 5, ranging between $\sim 0.01 - 0.05$ Mpc^{-3}. Therefore, with precise enough observational measurements, even the abundances of $\gtrsim 10^6$ $M_\odot$ BHs could potentially be used for constraining seed models. However, as we discuss in Section 4.2, possible degeneracies with signatures from other aspects of BH physics, such as accretion, dynamics, and feedback, may pose a significant challenge.

The current samples of local $\gtrsim 10^6$ $M_\odot$ SMBH populations are unlikely to be complete. Nevertheless, it has been possible to estimate the local BH mass functions (discussed in the next section) using the observed scaling relations between BH mass versus galaxy luminosities and stellar velocity dispersion, combined with the local galaxy luminosity and velocity functions (Marconi et al. 2004). The different estimates of the BH mass functions (Merloni & Heinz 2008; Shankar, Weinberg & Miralda-Escudé 2009; Cao 2010; Shen et al. 2020) in the literature have some spread that depends on the exact scaling relations they use (see Shankar et al. 2009 for details). We integrate these BH mass functions to obtain the number density of $\gtrsim 10^6$ $M_\odot$ BHs and show them as black data points in Fig. 4. Notably, the ESD model as well as the two intermediary DHS models produce local number densities that agree well with the latest observational constraints by Shen et al. (2020). The most restrictive DHS model (`SM5_LW10_LOWSPIN_RICH`) prediction is slightly lower than the

[4]All number densities are expressed in comoving units.

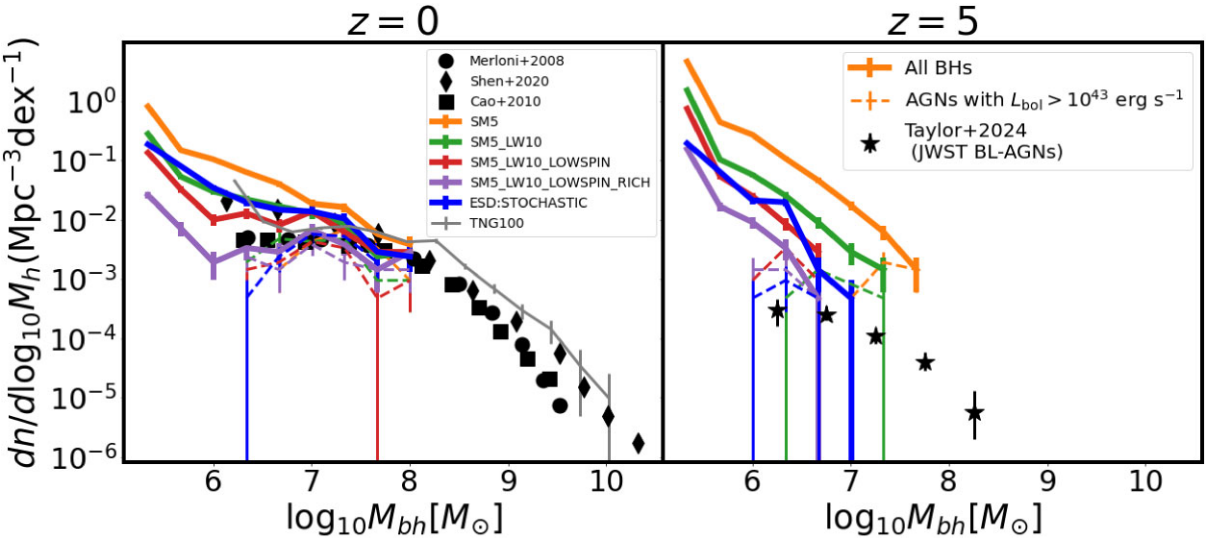

Figure 5. BH mass functions (solid lines) at $z = 0$ (left) and $z = 5$ (right) for the different seed models as compared to local observations (black data points) from Merloni & Heinz (2008), Cao (2010), Shen et al. (2020). At $z = 5$, we show the recent constraints from *J WST* BL-AGNs from Taylor et al. (2024); however, note that they only include active AGNs above the *JWST* detection limit. The dashed lines show the contributions from active BHs with $L_{\rm bol} > 10^{43}$ erg s^{-1}. The thin grey line shows the prediction from TNG100 simulation. At $z = 0$, the signatures of seeding are strongest for $\sim 10^5 - 10^6$ M$_\odot$ BHs. They persist at masses of $\sim 10^6 - 10^7$ M$_\odot$, but eventually disappear at $\gtrsim 10^7$ M$_\odot$. In contrast, at $z = 5$, the signatures of seeding exists at all BH masses ($\sim 10^5 - 10^8$ M$_\odot$) probed by our boxes.

estimate from Shen et al. (2020) by a factor of ~ 3, but is close to the estimates of Merloni & Heinz (2008) and Cao (2010). At the other end, the prediction of the most lenient DHS model (SM5) lies a factor of ~ 3 above the Shen et al. (2020) measurements. However, as we mentioned earlier, the uncertainties in these estimates may be significant as the scaling relations from which they are derived do not arise from a 'complete' population of local $\gtrsim 10^6$ M$_\odot$ SMBHs. With more precise estimates of the BH number densities in the future, we will be able to make a better assessment about which seed models are more viable than others.

3.3 BH mass functions

The left panel of Fig. 5 shows the BH mass functions (BHMFs) at $z = 0$ compared against the observational estimates for which the number densities were computed in the previous figure (Merloni & Heinz 2008; Cao 2010; Shen et al. 2020). As we already saw in Fig. 4, the seed model variations are the strongest for the lowest mass $\sim 10^5 - 10^6$ M$_\odot$ BHs. Recall again that for the DHS models, the smallest $\sim 10^5$ M$_\odot$ BHs are predominantly composed of local ungrown relics of seeds that formed at high-redshift ($z \sim 5 - 10$). The models start to gradually converge as we go from $\sim 10^6 - 10^7$ M$_\odot$, until they become similar to one another for $\gtrsim 10^7$ M$_\odot$ BHs. In fact, even the TNG100 simulation, which has a very different seed model ($\sim 10^6$ M$_\odot$ seeds are placed in $\sim 10^{10}$ M$_\odot$ haloes), predicts a very similar BHMF to the BRAHMA boxes at $\gtrsim 10^7$ M$_\odot$. All the seed models are also consistent with the observational BHMFs at $M_{\rm bh} \gtrsim 10^7$ M$_\odot$.

For $M_{\rm bh} \sim 10^6 - 10^7$ M$_\odot$ BHs, the comparison between our simulated and the observed BHMFs is naturally similar to what we saw in the BH number densities of $\gtrsim 10^6$ M$_\odot$ in Fig. 4. The most lenient DHS model is slightly higher than the latest Shen et al. (2020) BHMF and the most restrictive DHS model prediction is close to the measurements from Merloni & Heinz (2008) and Cao (2010) BHMF. The remaining models (ESD:STOCHASTIC, SM5_LW10, and SM5_LW10_LOWSPIN) are closest to the Shen et al. (2020) BHMF. Here again, we recall that in the absence of a complete population of local SMBHs down to $\sim 10^6$ M$_\odot$, these observational BHMFs may be subject to significant modelling uncertainties from the underlying BH–galaxy scaling relations they were derived from. We expect these measurements to converge in the future and potentially rule out some of our seeding scenarios (modulo uncertainties in BH accretion, dynamics, and feedback modelling).

Notably, the predicted seed model variations in the $z = 0$ BHMFs are qualitatively distinct compared to high-z BHMFs. While the $z = 0$ BHMFs for the different seed models converge at the massive end, the $z = 5$ BHMFs (right panel of Fig. 5) tend to have stronger seed model variations at the massive end. We also reported this in Bhowmick et al. (2024b) using lower mass seed models ($\sim 10^3$ M$_\odot$). The reason for the difference in behaviour at low-z versus high-z lies within the relative importances of the two distinct modes of BH growth; i.e. BH–BH mergers versus gas accretion.

In Fig. 6, we show the fraction of BH mass growth that occurs due to mergers (as a function of BH mass) for BH populations at redshifts 5, 3 & 0. At $z = 5$ (and higher redshifts), the BH growth is largely dominated by mergers, as also discussed in Bhowmick et al. (2024a, b, c). Our BH repositioning scheme is of course a significant caveat here as it corresponds to the most optimistic scenario for the merging efficiency. As mentioned earlier, we will investigate the relative contributions from mergers and accretion to the BH growth under subgrid dynamical friction in a follow-up paper. Another reason why mergers dominate over accretion is that in sufficiently low mass haloes, stellar feedback can readily prevent the gas from accumulating at the halo centres to fuel BH accretion. The $M_{\rm bh}^2$ scaling of the Bondi accretion rate also contributes to reduced accretion rates for seed BHs. At lower redshifts, the contribution from accretion becomes increasingly important particularly for higher mass BHs. At $z = 0$, accretion is the dominant contributor to BH growth for $\gtrsim 10^7$ M$_\odot$ BHs for all the seed models except the most lenient DHS model (where the contribution from mergers and

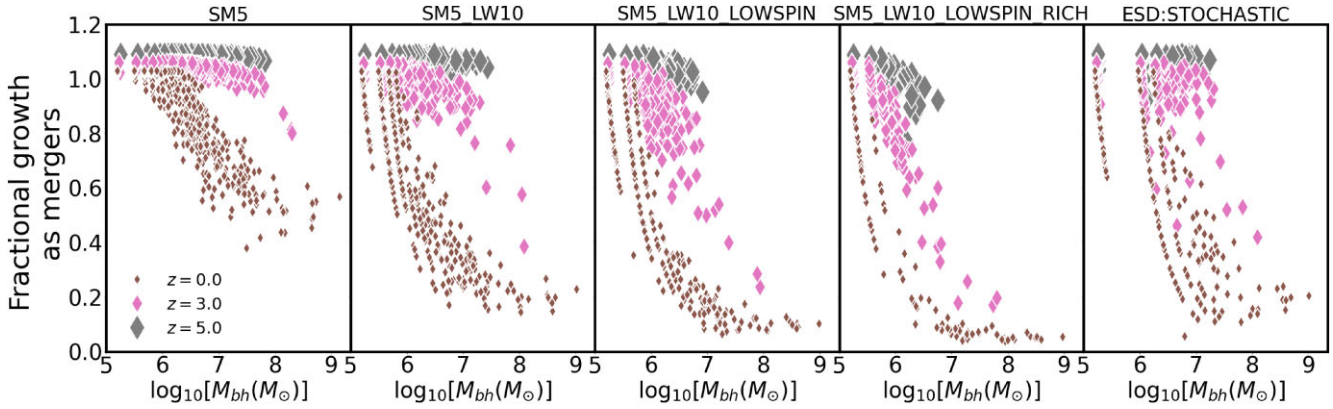

Figure 6. The fraction of the accumulated BH mass that is contributed via mergers (rather than gas accretion) is plotted as a function of BH mass. The different colours show BH populations at $z = 0$, 3, and 5 snapshots. We added artificial y-axis offsets for $z = 3$ and 5 for clarity. At $z = 5$ (and higher redshifts), BHs grow predominantly via mergers. The importance of accretion increases as we go to lower redshifts. Even at $z = 0$, the BH growth between $\sim 10^5$ and 10^6 $M_\odot$ is merger dominated. For more massive local BHs ($M_{\rm bh} \gtrsim 10^7$ $M_\odot$) however, accretion is the dominant contributor to the BH mass assembly. The signatures of seeding tend to most strongly persist in regimes wherein the mergers dominate BH growth. Accretion tends to erase signatures of seeding.

accretion are roughly equal). All that being said, when BHs grow via mergers, seed model variations tend to be stronger for more massive BHs (as in $z = 5$); this is because the merger-driven BH growth relies on the availability of seeds to fuel the mergers (that strongly depends on the underlying seed model). On the other hand, when BHs grow via gas accretion (as in $z = 0$), seed model variations tend to be weaker because accretion-driven BH growth relies on the availability of gas around the BH. In this case, only a select few BHs living in certain gas-rich environments will grow, regardless of the seed models.

Note also that even at $z = 0$, gas accretion is the dominant contributor to the BH mass assembly only for sufficiently massive $\gtrsim 10^7$ $M_\odot$ BHs. But at the low mass end of $\sim 10^5 - 10^6$ $M_\odot$, mergers continue to be the dominant mode of BH growth at $z = 0$. This explains why the signatures of BH seeding remain strong within $\sim 10^5 - 10^6$ $M_\odot$ all the way down to $z = 0$. Furthermore, the transition from merger-dominated growth at $\sim 10^5 - 10^6$ $M_\odot$ to accretion-dominated growth at $\gtrsim 10^7$ $M_\odot$ leaves a curious imprint on the $z = 0$ BHMFs. Specifically, the slope of the $z = 0$ BHMFs is somewhat steeper at $\sim 10^5 - 10^6$ $M_\odot$ compared to $\gtrsim 10^7$ $M_\odot$. This transition in slope does not occur for the $z = 5$ BHMFs wherein the entirety of BH growth is merger dominated. We also note that the commonly used Schechter function modelling of the $z = 0$ BHMFs would not be able to capture the steepening of the slope at $\sim 10^5 - 10^6$ $M_\odot$. To that end, if this transition in the $z = 0$ BHMF slope indeed occurs in the real Universe, a naive extrapolation of the observed BHMFs at $\gtrsim 10^6$ $M_\odot$ (which were indeed modelled based on Schechter functions) to lower masses, would underestimate the abundances of $\sim 10^5 - 10^6$ $M_\odot$ BHs.

To summarize our findings so far, the local $\sim 10^5 - 10^6$ $M_\odot$ BHs have strong signatures of seed models. This is because of two reasons. First, there is a substantial population of the lowest mass $\sim 10^5$ $M_\odot$ BHs at $z = 0$ that are ungrown relics of high redshift seeds ($z \sim 5 - 10$). Secondly, the BH growth from $\sim 10^5$ to $\sim 10^6$ $M_\odot$ is dominated by mergers all the down to $z \sim 0$. This merger-driven growth tends to retain the signatures of seed models in the abundances of $\sim 10^5 - 10^6$ $M_\odot$ BHs. However, as accretion-driven growth becomes increasingly important for higher mass BHs, the signatures of seeding begin to be erased and eventually disappear for $\gtrsim 10^7$ $M_\odot$ BHs.

During the writing of this paper, Taylor et al. (2024) published BH mass functions for broad-line (BL) AGNs at $z \sim 4 - 6$ detected using *JWST* (shown as black stars in right panel of Fig. 5), probing down to BH masses of a few $10^6 M_\odot$. While the comparison against *JWST* observations was the focus of our previous paper (Bhowmick et al. 2024c), it is instructive to take a detour and compare these recent results with our simulation predictions, before bringing back our focus on $z = 0$. Most of our overall $z = 5$ BHMFs are significantly higher than these observations (black stars versus solid lines in Fig. 5). However, like any study that relies on detecting BH via their accretion signatures, Taylor et al. (2024) only probes BHs that have luminosities above the detection limit, so they can be considered lower limits in a sense. Notably, our simulated BHMFs of active BHs (above $L_{\rm bol} > 10^{43}$ erg s^{-1}, dashed lines in Fig. 5) are substantially lower than the overall BHMFs, and are much closer to the observational constraints. All this is again tied to the fact that the BH mass assembly at high-z is merger dominated at the low BH-mass end in our simulations. If this is true in the real Universe, we could expect the existence of a much larger population of inactive merging BHs that cannot be probed by *JWST*. The *JWST* based measurements of Taylor et al. (2024) would then serve as a strict lower limit to the overall BHMFs at high-z. Future facilities such as LISA will be able to test for the possible existence of a population of lower luminosity merging BHs.

3.4 AGN luminosity functions

The first three columns of Fig. 7 show the AGN luminosity functions (LFs) close to the local Universe; i.e. $z \sim 0 - 0.4$. We show both the bolometric luminosities as well as the X-ray luminosities. Note that while the simulations are able to readily predict the bolometric luminosities from the accretion rates (modulo the uncertainties in the accretion and feedback model), they require a bolometric correction to infer the X-ray luminosities. Conversely, while the observations are able to directly measure the X-ray luminosities (barring uncertainties due to obscuration and X-ray binary contributions), they require a bolometric correction to infer the bolometric luminosities. Here we use the bolometric correction from Shen et al. (2020).

For sufficiently bright AGNs ($L_{\rm bol} > 10^{43}$ erg s^{-1} and $L_{2-10\ \rm keV} > 10^{42}$ erg s^{-1}), the LFs for all the different seed models converge. The

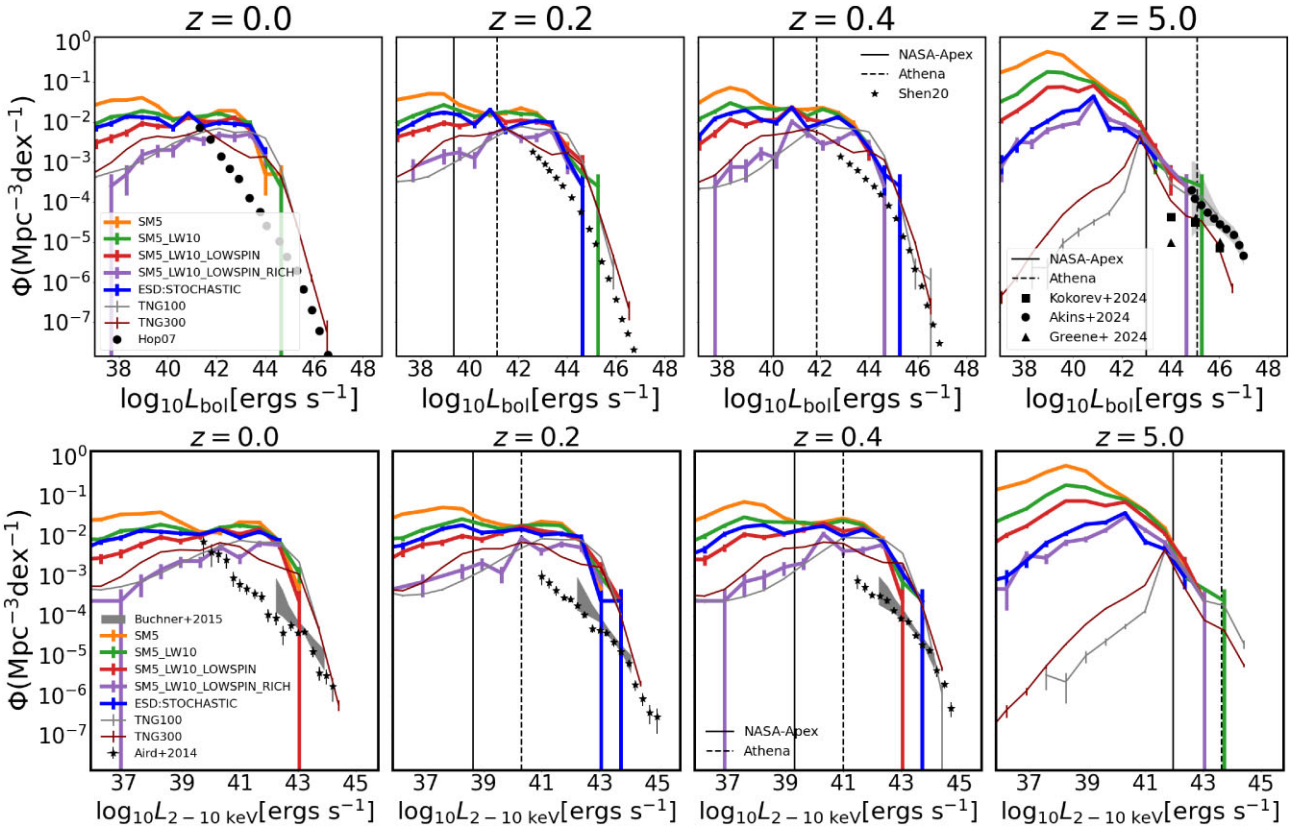

Figure 7. The top and bottom rows show the AGN bolometric and hard X-ray luminosity functions respectively, for the different seed models. The left three columns show different redshifts in the nearby Universe whereas the rightmost column shows the $z = 5$ prediction. The thin grey and maroon lines show predictions TNG100 and TNG300, respectively. The black points correspond to observational constraints from Shen et al. (2020), Aird et al. (2015), and Buchner et al. (2015). All the seed models converge at $L_{2-10\ \mathrm{keV}} \gtrsim 10^{42}$ erg s^{-1} or $L_{\mathrm{bol}} \gtrsim 10^{43}$ erg s^{-1}. The strongest seed model variations in the AGN LFs are at $L_{\mathrm{bol}} \lesssim 10^{40}$ erg s^{-1} and $L_{2-10\ \mathrm{keV}} \lesssim 10^{39}$ erg s^{-1}. With proposed X-ray facilities such as AXIS, these luminosities can be accessible in the local Universe, but not in the high-z Universe.

`Illustris-TNG` seed model also produces similar LFs to the `BRAHMA` boxes in this regime (see thin maroon and grey lines). The abundances of the brightest quasars ($L_{\mathrm{bol}} > 10^{45}$ erg s^{-1} or $L_{2-10\ \mathrm{keV}} > 10^{44}$ erg s^{-1}), probed only by the much larger TNG boxes, are broadly consistent with observations. However, for AGNs with $L_{\mathrm{bol}} \lesssim 10^{44}$ erg s^{-1}, all the simulated LFs are greater than the observations by a factor of ~ 10. This was also identified in previous works (Weinberger et al. 2018; Bhowmick et al. 2021). The same is true for several other simulations in the literature (see fig. 5 of Habouzit et al. 2022). Recall from the previous section that the local BHMFs exhibit much better agreement between the simulations and observations (particularly for $\gtrsim 10^7$ M$_\odot$ BHs). This is because the local BHMFs are derived from BH–galaxy scaling relations and the galaxy luminosity functions, both of which are reasonably well reproduced by the Illustris-TNG galaxy formation model upon which `BRAHMA` is based (Terrazas et al. 2020; Vogelsberger et al. 2020b). The agreement in the BHMFs between the simulations versus observations hints that at least part of the discrepancy in AGN LFs may be contributed by AGN obscuration. The uncertainties in the bolometric corrections as well as modelling uncertainties in the accretion prescription can also play a significant role. In any case, our seeding prescriptions are not consequential to this discrepancy. Therefore, we defer a detailed investigation of this discrepancy to a future paper.

Despite the current tension with the observed $z = 0$ LFs, the simulation predictions for the different seed models help us identify AGN populations wherein there are strong signatures of seeding. The seed model variations in AGN LFs become strong at $L_{\mathrm{bol}} \lesssim 10^{40}$ erg s^{-1} and $L_{2-10\ \mathrm{keV}} \lesssim 10^{39}$ erg s^{-1}. For example, the differences between the LF predictions for `SM5` and `SM5_LW10_LOWPSIN_RICH` boxes become larger than factors of ~ 100 at these faint luminosities. While these luminosities are substantially below what the current observations probe, they may be accessible by proposed X-ray facilities such as Athena (Barret et al. 2020) and the Advanced X-ray Imaging Satellite or AXIS (Reynolds et al. 2023). In particular, AXIS could potentially detect AGNs all the way down to a few times $\sim 10^{38}$ erg s^{-1} in the local Universe. Below those luminosities, X-ray binaries are expected to become a substantial source of contamination (Gallo et al. 2023).

Finally, we compare our local AGN LFs to that at $z = 5$ shown in the rightmost column of Fig. 7. The seed model variations at $z = 5$ exhibit a similar trend to that at $z = 0$; i.e. smaller variations at the brightest end ($L_{2-10\ \mathrm{keV}} \gtrsim 10^{43}$ erg s^{-1}) and larger variations at the faint end ($L_{2-10\ \mathrm{keV}} \lesssim 10^{39}$ erg s^{-1}). Therefore, both $z = 5$ and $z = 0$ LFs have a similar luminosity range of $L_{2-10\ \mathrm{keV}} \lesssim 10^{39}$ erg s^{-1} wherein we expect signatures of seeding. However, these luminosities inaccessible at $z \sim 5$ even with future X-ray facilities. The recent *JWST* observations of high-z AGN (black points in Fig. 7) also only

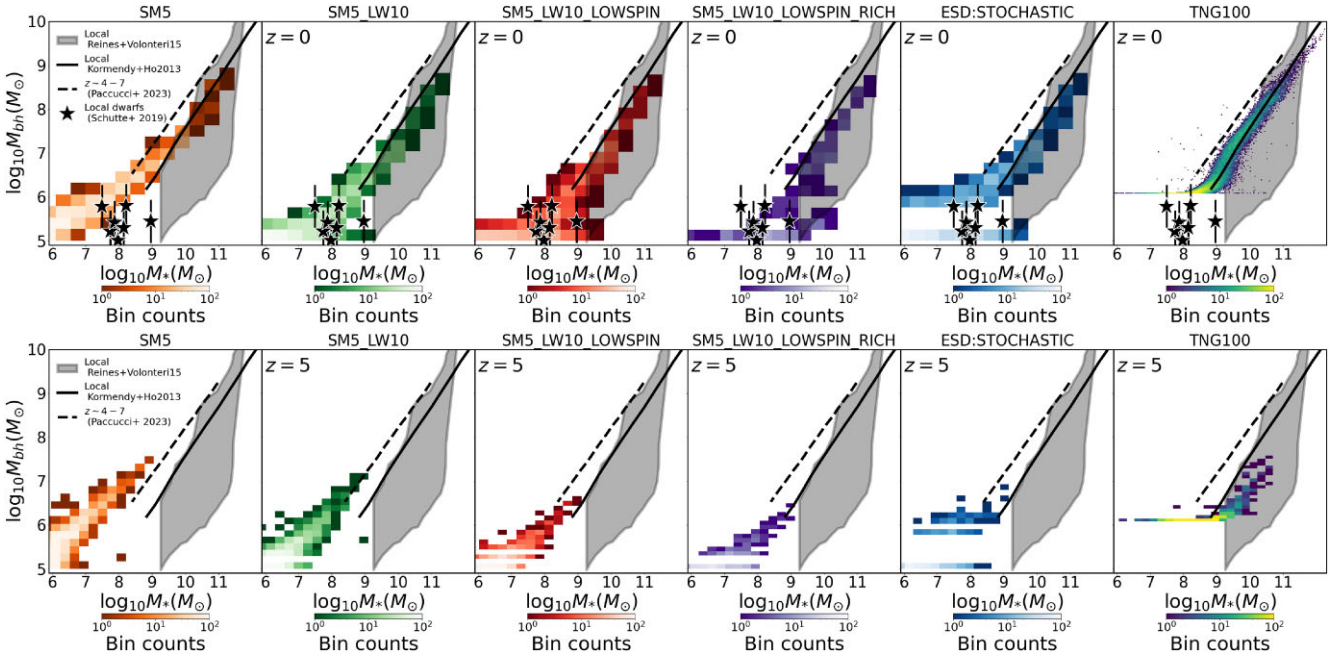

Figure 8. M_* versus $M_{\rm bh}$ relation predictions for our different BH seed models compared against different observational measurements. Specifically, we plot the total stellar mass of the subhaloes versus the mass of central (most massive) BH. The four left panels show the DHS models. The fifth panels shows the ESD model. The rightmost panels show the results from TNG100. The top rows show the local scaling relations compared against observations for $\gtrsim 10^6$ M$_\odot$ BHs from Kormendy & Ho (2013) (black solid line) and Reines & Volonteri (2015) (shaded region), as well as $\sim 10^5 - 10^6$ M$_\odot$ BHs within dwarf galaxies from Schutte et al. 2019 (black stars). The bottom row shows the high-z ($z = 5$) scaling relation compared against the relation derived by Pacucci et al. 2023 (black dashed line) for *JWST* AGNs at $z \sim 4 - 7$. The different columns show the different seed models. For local galaxies with $M_* \gtrsim 10^{10}$ M$_\odot$, all the seed models produce similar M_* versus $M_{\rm bh}$ relations that are also consistent with observations. However, for local dwarf galaxies ($M_* \lesssim 10^9$ M$_\odot$), the M_* versus $M_{\rm bh}$ relations have significant seed model variations. Compared to the Schutte et al. (2019) measurements, the most optimistic DHS model (`SM5`) predictions are higher, while the remaining seed models are broadly consistent.

probe down to $L_{\rm bol} \sim 10^{44}$ erg s^{-1} at $z \sim 4 - 6$, where the LFs are similar for all the seed models. As discussed in our previous paper (Bhowmick et al. 2024c), our simulations are in broad agreement with the *JWST* LFs at $z \sim 5$ (albeit the observations currently have substantial uncertainties).

We see yet another striking difference in the seed model variations amongst the *overall* BH versus the *active* AGN populations at $z = 0$ and $z = 5$. At $z = 0$, the seed model variations in the AGN LFs showed a similar trend to the BHMFs; i.e. seeding signatures become weaker for more massive BHs as well as more luminous AGNs at $z = 0$. But at $z = 5$, the abundances of the most luminous AGNs have no seed model variations whereas that of the most massive BHs have the strongest seed model variations. The reason for all this goes back to the mergers versus accretion-dominated BH growth at various redshifts shown in Fig. 6. At $z = 5$, the BHMFs are 'de-coupled' from the 'AGN LFs' due to the merger-dominated BH growth. In such a case, only a select set of BHs end up in environments with enough fuel to become luminous AGN regardless of the seed model. However, the formation of massive BHs at $z = 5$ relies only on the availability of sufficient seeds. In contrast, close to $z = 0$, gas accretion predominantly drives the growth of massive $\gtrsim 10^7$ M$_\odot$ BHs. Therefore, at $z = 0$, the BHMFs are 'coupled' to the AGN LFs, such that the formation of massive BHs essentially depends on the availability of accreting gas rather than the number of seeds.

Overall, while we concluded in previous works (Bhowmick et al. 2021, 2024a, c) that AGN observations at higher-z ($z \sim 5 - 10$) may not be very informative about seed models, the same is not true in the local Universe. Somewhat counterintuitively, the local AGN LFs have a better prospect of constraining seed models compared to the higher-z AGN LFs. But this is simply because in the local Universe, future X-ray missions have the ability to probe exceptionally low X-ray luminosities (down to $\sim 10^{38}$ erg s^{-1}) wherein our simulations show strong signatures of seeding.

3.5 Stellar mass versus BH mass scaling relations

We now focus on the relation between the BHs and their host galaxies at $z = 0$. In the top panels of Fig. 8, we show the local stellar mass versus BH mass (M_* versus $M_{\rm bh}$) relations for the different seed models, compared against the observations. We note that our simulations are not large enough to robustly probe the scatter of the M_* versus $M_{\rm bh}$ relations (particularly in higher mass galaxies) as revealed in the observational measurements. This is because in these volumes, it is difficult to form (rarer) BHs that are significantly further away from the mean relation. Nevertheless, the simulations do capture the mean M_* versus $M_{\rm bh}$ relations for the different seed models, which we can compare against observations. For $\gtrsim 10^9$ M$_\odot$ galaxies, the M_* versus $M_{\rm bh}$ relations are similar for all the seed models; these predictions are also in good agreement with measurements from Kormendy & Ho (2013) and Reines & Volonteri (2015). Notably, these galaxies host $\gtrsim 10^7$ M$_\odot$ BHs wherein the majority of the mass growth occurs via gas accretion in our simulations.

For dwarf galaxies ($\lesssim 10^9$ M$_\odot$) that typically host BHs between $\sim 10^5 - 10^7$ M$_\odot$, the M_* versus $M_{\rm bh}$ relations exhibit non-negligible seed model variations. For the most lenient DHS model (`SM5`), the slope of the scaling relations in $M_* \lesssim 10^9$ M$_\odot$ galaxies becomes slightly shallower than that in $M_* \gtrsim 10^9$ M$_\odot$ galaxies. This is due to

the strong merger-driven growth of BHs in $M_* \lesssim 10^9$ M$_\odot$ galaxies, fuelled by the greater availability of seeds. For the more restrictive DHS models, there are fewer seeds to fuel merger-driven growth in $M_* \lesssim 10^9$ M$_\odot$ galaxies. This leads to smaller BH masses (at fixed stellar mass) in $M_* \lesssim 10^9$ M$_\odot$ galaxies compared to the more lenient DHS models. Therefore, for the SM_LW10_LOWSPIN and SM_LW10_LOWSPIN_RICH DHS models, the change in slope of the scaling relations between $M_* \gtrsim 10^9$ M$_\odot$ and $M_* \lesssim 10^9$ M$_\odot$ is less prominent compared to the SM5 model. Lastly, the ESD model shows a somewhat larger scatter in the M_* versus $M_{\rm bh}$ relations for $M_* \lesssim 10^9$ M$_\odot$ galaxies, compared to the DHS models. This may be because in the ESD seed model, the $\sim 10^5$ M$_\odot$ BHs are descendants of unresolved lower mass seeds that presumably went through a diverse range of (merger-driven) growth histories; we shall investigate this further in the future using larger volume simulations that will be able to quantify the scatter more robustly.

We can now compare our predictions in the dwarf galaxy regime to observations from Schutte et al. (2019), (black stars in Fig. 8). The most lenient SM5 model generally predicts $\sim 5-10$ times higher BH masses in $M_* \lesssim 10^9$ M$_\odot$ galaxies compared to the observations. The remaining seed models are broadly consistent with the observations. These results demonstrate that in the future when the sample sizes are larger and measurement uncertainties are smaller, we might be able to discriminate between seeding scenarios based on the M_* versus $M_{\rm bh}$ relations of BHs in local dwarf galaxies. However, to be able to do so, we also need to understand the impact of BH accretion, dynamics, and feedback modelling in this regime; we will address this in future work.

The bottom panels of Fig. 8 shows the M_* versus $M_{\rm bh}$ relations at $z = 5$ (which was the focus of our previous paper Bhowmick et al. 2024c). In contrast to $z = 0$ where the seed models impact the M_* versus $M_{\rm bh}$ relations only in the dwarf galaxy regime, the $z = 5$ relations are significantly impacted even in the most massive galaxies (and BHs) probed by our simulation volumes (i.e. $M_* \sim 10^{10}$ M$_\odot$). This again, is because mass growth is dominated by mergers for all the BHs at $z = 5$ (and higher redshifts). Based on recent observations with *JWST*, Pacucci et al. (2023) inferred an intrinsic M_* versus $M_{\rm bh}$ relation (black dashed line) that is overmassive compared to the local scaling relations by $> 3\sigma$. Our intermediary DHS models (SM5_LW10 and SM5_LW10_LOWSPIN) and the ESD model produce the best agreement with the inferred high-z relations. It is noteworthy that these are also the same models which produce the best agreement with the most recent observational estimates of the local BH mass functions at $M_{\rm bh} \lesssim 10^7$ M$_\odot$ (Shen et al. 2020, revisit Fig. 5) as well as the observed $M_{\rm bh}$ to M_* ratios for the local dwarf galaxies (top panels of Fig. 8). On the other hand, the SM5 model that overestimates the high-z M_* versus $M_{\rm bh}$ relations, also slightly overestimates the local BH mass functions at $M_{\rm bh} \lesssim 10^7$ M$_\odot$ (and also the $M_{\rm bh}$ to M_* relations for local dwarf galaxies). Likewise, the SM5_LW10_LOWSPIN_SPIN model that underestimates the high-z M_* versus $M_{\rm bh}$ relations, also tends to be at the lower end of the different observed local BHMFs at $M_{\rm bh} \lesssim 10^7$ M$_\odot$. In other words, the seeding models that have the best agreement with the inferred high-z $M_* - M_{\rm bh}$ relation using *JWST*, also produce good agreement with the existing local observations. While the current observational uncertainties are relatively large, it is encouraging to see that three of our seed models are simultaneously consistent with current observations of BHs at high-z as well as in the local Universe.

Lastly, we can also compare the BRAHMA predictions to those of TNG100, shown in the rightmost panels of Fig. 8. We notice that unlike the BRAHMA boxes, the TNG100 scaling relations flatten (zero slope) at their adopted seed mass of $\sim 10^6$ M$_\odot$ in the dwarf galaxy regime of $M_* \lesssim 10^9$ M$_\odot$. Essentially, this is because there are not enough seeds produced in TNG100 to fuel merger-driven BH growth within $M_* \lesssim 10^9$ M$_\odot$ galaxies wherein gas accretion is suppressed by stellar feedback. Concurrently, due to the lack of merger-driven BH growth, the TNG100 scaling relations help us easily visualize the fact that at both $z = 0$ and 5, accretion-driven BH growth starts to be significant only when the stellar mass exceeds $M_* \gtrsim 10^9$ M$_\odot$. This explains why our BRAHMA boxes do not see substantial accretion-driven BH growth at $z = 5$, as they are too small to produce $M_* \gtrsim 10^9$ M$_\odot$ galaxies at these redshifts. At $z = 0$ however, $M_* \gtrsim 10^9$ M$_\odot$ galaxies become common enough to be captured by our BRAHMA boxes, and we readily see accretion-driven BH growth.

3.6 BH occupation fractions

The BH occupation fractions in local dwarf galaxies is regarded as one of the most promising observables to constrain seed models in the local Universe. The local BH occupation fractions for our different simulations are shown in Fig. 9 for different BH mass thresholds. The left panels show the smallest threshold we can probe in our simulations; i.e. $\gtrsim 10^5$ M$_\odot$. We find that the occupation fractions for $\gtrsim 10^5$ M$_\odot$ BHs are substantially different between the different seed models for $M_* \lesssim 10^9$ M$_\odot$ galaxies. For $\sim 10^9$ M$_\odot$ galaxies, the most lenient DHS model predicts an occupation fraction of ~ 100 per cent whereas the most restrictive DHS model predicts ~ 40 per cent occupation fractions. The ESD model predicts occupation fractions ~ 70 per cent in $\sim 10^9$ M$_\odot$ galaxies. The seed model variations are stronger for even lower mass galaxies.

Much like the BH mass functions, the seed model variations seen in the BH occupation fractions also tend to become smaller for increasing BH masses. However, even for $\gtrsim 10^6$ M$_\odot$ BHs, the BH occupation fractions in our simulations show significant seed model variations. For the $M_* \sim 10^9$ M$_\odot$ galaxies, the BH occupation fractions vary from 20 per cent to 100 per cent from the most restrictive to the most lenient DHS model. For even higher mass thresholds of $M_{\rm bh} \gtrsim 10^7$ M$_\odot$ (right panels of Fig. 9), all of our seed models predict broadly similar results.

3.6.1 *Comparison with observations*

Several attempts have been made to observationally constrain the BH occupation fractions, which we compare to our simulations in the top panels of Fig. 9. Some of the early measurements were made by Greene (2012) using X-ray AGN samples from Desroches et al. (2009) and Gallo et al. (2010). However, since these measurements only target *active* AGNs, one needs to make assumptions for the AGN fractions (fraction of BHs that are active and detectable) in order to infer the occupation fractions of the full BH population (active as well as inactive). By assuming 10 per cent detectable AGN fractions, and counting only BHs that are above Eddington ratios of 10^{-4}, Greene (2012) derived the occupations fractions of $> 3 \times 10^5$ M$_\odot$ and $> 10^6$ M$_\odot$ BHs (black circles and squares in the top-middle panel). A few years later, Miller et al. (2015) used a similar procedure on a much larger sample of X-ray AGNs and inferred the active as well as the full BH occupation fractions (black squares and grey region respectively in the top-left panel). Since our simulated AGN LFs are currently higher than the observed LFs at the faint end (revisit Fig. 7), it is difficult to replicate the selection criteria used in these works and perform an even-handed comparison between simulated and observed occupation fractions. Nevertheless,

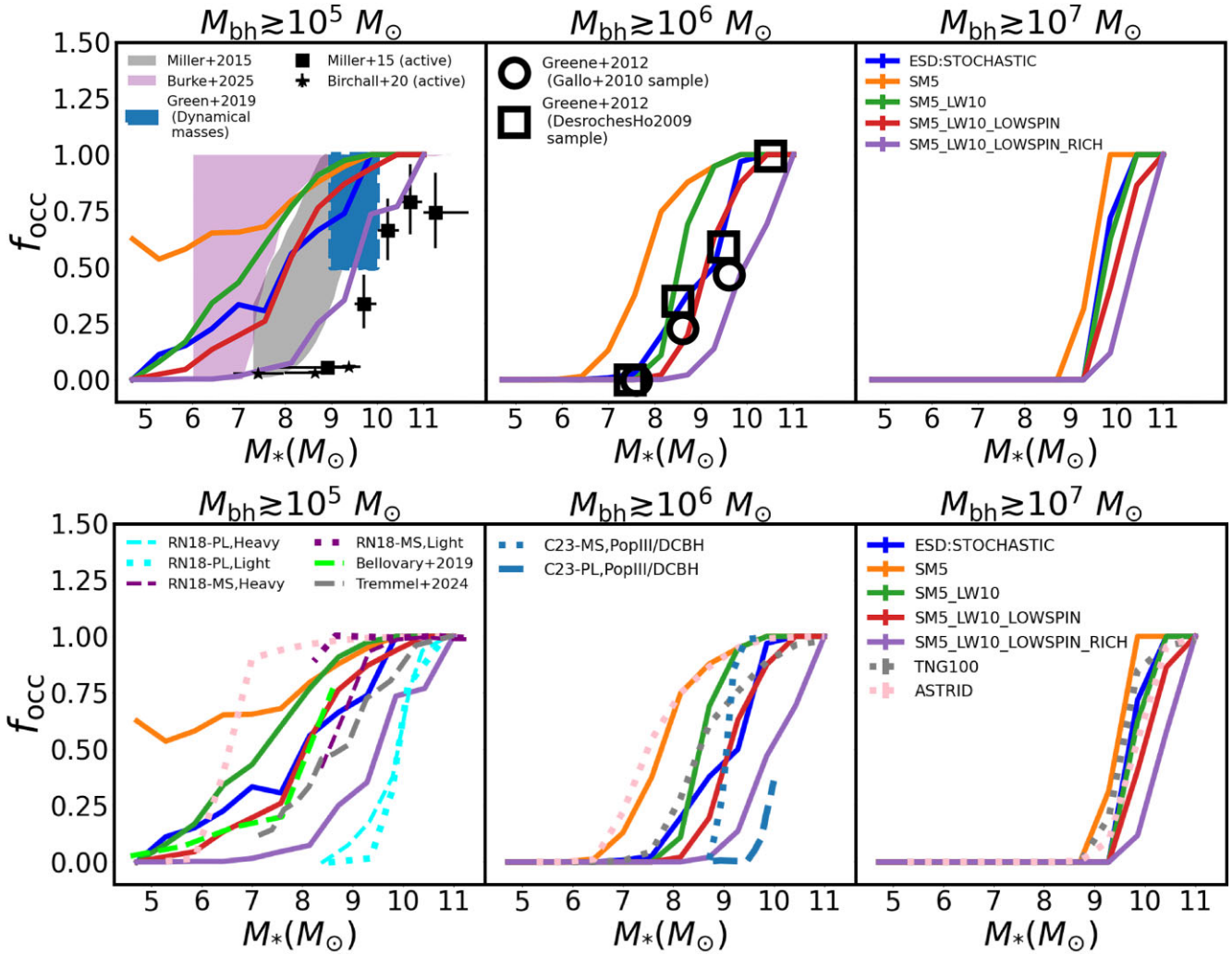

Figure 9. $z = 0$ occupation fractions predicted by the different seed models. The different columns correspond to BH samples with different mass thresholds. We compare our predictions with observational constraints in the top row. The black open squares and circles in the middle panels are the early measurements from Greene (2012) based on samples of Desroches, Greene & Ho (2009) and Gallo et al. (2010), respectively. The black squares in the left panels are observational measurements of the active BH occupation fractions from Miller et al. (2015), along with the grey region being their inferred overall occupation fraction. The purple shaded region corresponds to the most recent constraints (lower limits) for the overall occupation fraction by Burke et al. (2025). The blue region derived by Greene et al. (2020) corresponds to the only constraints that are derived from dynamical mass measurements of a sample of 10 BHs in Nguyen et al. (2019). The bottom row compares our simulations with several other theoretical models. The dashed bright green and grey lines are hydrodynamic simulations of Bellovary et al. (2019) and Tremmel et al. (2024), respectively. Purple and cyan dashed and dotted lines in the second panel are predictions from the semi-analytical model of Ricarte & Natarajan 2018 (R18). The blue dashed and dotted lines are predictions from Chadayammuri et al. (2023) using the semi-analytic model of R18. The grey and pink dotted lines are predictions from `TNG100` and `ASTRID`, respectively. Seed model variations are substantial for $\gtrsim 10^5$ $M_\odot$ and $\gtrsim 10^6$ $M_\odot$ BHs. Our predictions are broadly consistent with observations, with current uncertainties being too large to discriminate between seeding scenarios.

at the very least, it is encouraging to see that the Greene (2012) and Miller et al. (2015) results broadly fall within the range of our simulation predictions for the different seed models. Additionally, the active occupation fractions from Miller et al. (2015) and Birchall, Watson & Aird (2020) (black squares and stars respectively in the top-left panel) serve as lower limits to the overall BH occupation; they also do not rule out any of our seed models since all of the simulations predict higher overall BH occupations compared to their results. Very recently, Burke et al. (2025) derived multiwavelength constraints for the overall BH occupation fraction by combining X-ray, radio, and optical variability data (pink shaded region in the top-left panel). Their lower limits for the occupation fractions are higher than our two restrictive DHS models. However, they are not in conflict with the predictions of our optimistic DHS models. The Burke et al. (2025) constraints are also higher than our ESD model predictions; this is not surprising because their constraints do not assume a specific BH mass threshold, whereas we do not explicitly resolve the low mass seeds that the ESD model attempts to represent.

The most even-handed comparison for our $M_{bh} > 10^5$ $M_\odot$ occupation fractions would be against the results from Greene et al. (2020), as they used dynamical BH mass measurements (Nguyen et al. 2019) to estimate the occupation fraction of $M_{bh} \gtrsim 10^5$ $M_\odot$ BHs in a sample of $\sim 10^9 - 10^{10}$ $M_\odot$ (albeit only for 10 galaxies). Based on BH detections in at least 5 out of 10 galaxies, Greene et al. (2020) inferred > 50 per cent occupation fractions for $\gtrsim 10^9$ galaxies; this is also consistent with all of our seed model predictions

(see blue region in the top-left panel of Fig. 9). In summary, the current measurements for the BH occupation fractions have too large uncertainties to strongly constrain our seed models. Future measurements with deeper X-ray probes like Athena and AXIS (see Gallo et al. 2023), along with large sample of dynamically measured BH masses in dwarf galaxies, are going to be crucial for constraining seed models using local BH occupation fractions.

3.6.2 Comparison with other model predictions

We also compare our predicted BH occupation fractions with those of several other simulations and semi-analytic models in the bottom panels of Fig. 9. We start with cosmological hydrodynamic simulations. Bellovary et al. (2019) and Tremmel et al. (2024) (ROMULUS) use a similar seed model originally developed in Tremmel et al. (2017) wherein heavy $\sim 10^5$ $M_\odot$ seeds are generated from individual gas cells that are high density (~ 15 times the SF threshold), low metallicity ($\lesssim 3 \times 10^{-4}$), and have temperatures between $9500 - 10\,000$ K. Their occupation fractions of $\geq 10^5$ $M_\odot$ BHs (bottom-left panel) are smaller than our most optimistic DHS model (SM5) likely because they adopt a much higher gas density threshold for seed formation compared to ours. However, due to the addition of LW flux, gas spin, and halo environment criteria, our most pessimistic DHS model (SM5_LW10_LOWSPIN_RICH) predicts BH occupations smaller than these works. The intermediary DHS models (SM5_LW10 and SM5_LW10_LOWSPIN) and the ESD models produce BH occupation fractions broadly similar to Bellovary et al. (2019).

The ASTRID (Ni et al. 2022; Ni et al. 2024) simulation initializes BHs with a power-law distribution of seed masses from 4.4×10^4 to 4.4×10^5 $M_\odot$ in haloes exceeding total masses of 7.4×10^9 $M_\odot$ and stellar masses of 3×10^6 $M_\odot$. The simulation has been so far run to $z = 0.2$ with galaxy catalogues processed down to $z = 0.4$ (Chen et al., in preparation). While it has not yet reached $z = 0$, it is nevertheless insightful to compare the $z = 0.4$ occupation fractions against our local results (using data obtained by private communication). For $\gtrsim 10^5$ $M_\odot$ BHs, the ASTRID occupation fractions are higher than all of our seed models within $M_* \gtrsim 3 \times 10^6$ $M_\odot$ galaxies. However, due to the adopted stellar mass threshold, the occupation fractions sharply fall off in galaxies with $M_* \lesssim 3 \times 10^6$ $M_\odot$. For $\gtrsim 10^6$ $M_\odot$ BHs, the ASTRID occupation fractions are similar to our most optimistic SM5 seed model.

The IllustrisTNG simulations seed $\sim 10^6$ $M_\odot$ BHs in 7×10^{10} $M_\odot$ haloes. The relatively high halo mass threshold makes the TNG seed model substantially more restrictive than the SM5 model. Therefore, despite the lower seed mass than BRAHMA, TNG predicts smaller occupation fractions for $\gtrsim 10^6$ $M_\odot$ BHs compared to the SM5 model. However, the TNG predictions are higher than the SM5_LW10_LOWSPIN_RICH model. For the highest mass $\gtrsim 10^7$ $M_\odot$ BHs, the BRAHMA, IllustrisTNG as well as the ASTRID simulations predict broadly similar occupation fractions. This adds further support to our finding that for $\gtrsim 10^7$ $M_\odot$ BHs, the signatures of seeding are largely erased.

A general takeaway from the above results is that the BH occupation fractions predicted by BRAHMA span a broad range, within which the predictions from many previous hydrodynamic simulations fall comfortably. This serves as a demonstration of the diversity of the seed models explored within the BRAHMA simulations, some of which are significantly more lenient compared to other simulations in the literature, while others are significantly more restrictive.

The semi-analytic model of Ricarte & Natarajan (2018)(hereafter R18) has been used to predict BH occupation fractions for different seeding and growth scenarios (R18; Chadayammuri et al. 2023). Their predictions for $\gtrsim 10^5$ $M_\odot$ BHs are also shown in the bottom left panels of Fig. 9. These papers explored a 'Heavy' seed model with a seed mass distribution that peaks at $\sim 10^5$ $M_\odot$, using the seeding criteria from Lodato & Natarajan (2006) (which is essentially our *gas-spin criterion*). They also explore a 'light' seed model which assumes a power-law seed mass distribution from 30 to 100 $M_\odot$. R18 finds that their occupation fractions are also sensitive to the accretion scenario. Therefore, in order to interpret the differences between R18 versus BRAHMA, we have to also account for the differences in the BH accretion models. R18 has two distinct modes of accretion, an episodic 'burst' mode and a 'steady' mode. At $z \gtrsim 2$, their accretion is mainly dominated by the 'burst mode', where for every major merger (merging halo mass ratios > 0.1) the BHs are grown at the Eddington rate until they reach a cap that corresponds to the local $M - \sigma$ relation. As already seen in Fig. 6, the BRAHMA simulations do not predict any significant contribution from BH accretion on to the BH growth at $z \gtrsim 3$. This essentially means that the episodic burst mode assumed by R18 is absent in BRAHMA. In the 'steady' accretion mode that is more significant at $z \lesssim 2$, R18 adopts a 'main sequence' (MS) accretion model wherein the BH accretion rates are proportional to (a thousandth) of the star formation rates. This mode allows for significantly faster growth of BHs in low mass haloes compared to the BRAHMA simulations. Additionally, they also adopt a 'power-law' (PL) model wherein the Eddington ratios are drawn from a power-law distribution. This model exhibits slower growth of BHs in low mass haloes, consistent with BRAHMA. All that being said, the most even-handed comparisons with the BRAHMA seed models would be with those R18 seed models that are coupled with the PL accretion model. We can see that for all the PL models (cyan lines in the bottom-left panel of Fig. 9), the R18 occupation fractions are smaller than all the BRAHMA boxes. This is likely because R18 allows seed formation to occur only between $z \sim 15 - 20$, whereas the seed formation rates in BRAHMA are suppressed only after $z \sim 10$. Since the MS models of R18 allow for faster BH accretion in low mass haloes, they predict higher occupation fractions compared to the PL models. As a result, the MS model predictions of R18 lie within the span of our BRAHMA predictions despite their seed models being more restrictive.

To summarize, we find that the BH occupation fractions in local dwarf galaxies contain strong imprints of seeding, with predicted seed model variations for $\gtrsim 10^5$ $M_\odot$ and $\gtrsim 10^6$ $M_\odot$ BHs ranging from $\sim 40 - 100$ per cent and $\sim 20 - 100$ per cent, respectively for $M_* \sim 10^9$ $M_\odot$ galaxies. However, other studies such as R18 and Chadayammuri et al. (2023) have shown that they may also be sensitive to the BH accretion modelling. In the future, we plan to explore the dependence of BH occupation fractions on different choices for accretion models.

4 DISCUSSION

4.1 Feasibility of low mass seeds and heavy seeds as origins of the local SMBH populations

We now discuss the feasibility of low mass seeds versus heavy seeds in explaining the local SMBH populations in the context of our results. When we look at the different local BH observables in Figs 4 to 9, we find that the ESD model predictions are in good broad agreement with their observational counterparts, particularly for the abundances of $10^6 - 10^7$ $M_\odot$ and the $M_* - M_{\rm bh}$ relations in dwarf

galaxies. This suggests that the lower mass $\sim 10^3$ $M_\odot$ seeds may be viable origins for the local SMBH populations. While our ESD model is agnostic as to which physical low mass seeding scenarios it represent, it is worth noting that the target seed masses of $\sim 10^3$ $M_\odot$ best resemble NSC seeds or extremely massive Pop III seeds.

As for the DHS models, there is a significant spread in predictions at the lowest mass end $\sim 10^5 - 10^6$ $M_\odot$ that is primarily composed of local ungrown relics of seeds that form at high redshift ($z \sim 5 - 10$). The most lenient `SM5` model predicts number densities and BHMFs slightly above the upper end of the observational measurements. While the BHMF estimates can be impacted by uncertainties in the BH–galaxy scaling relations, the `SM5` model also overpredicts the $M_{\rm bh}/M_*$ ratios in the dwarf galaxy regime compared to measurements of Schutte et al. (2019). All this is not surprising because `SM5` assumes that every halo with sufficient dense and metal-poor gas will form DCBHs; this is likely to be too optimistic as we expect the need for additional conditions to prevent cooling and fragmentation. When we add the *LW flux criterion* and the *gas spin criterion*, the resulting BH number densities, BHMFs and $M_{\rm bh}/M_*$ ratios are broadly consistent with observations. However, the relatively low value of 10 J_{21} for the critical LW flux may only be feasible when there is additional help from dynamical heating (e.g. in major halo mergers Wise et al. 2019; Regan et al. 2020a) in preventing H_2 cooling and fragmentation. For this reason, we added an additional criterion in `SM5_LW10_LOWSPIN_RICH` that requires DCBH formation to occur only in rich environments with neighbouring massive haloes. For this most restrictive DHS model, the predicted BH number densities and BHMFs are already at the lower end of the observed measurements (revisit Figs 4 and 5); the predicted BH occupation fractions are also below the latest lower limits derived by Burke et al. (2025). These results imply that any DCBH formation mechanism that is substantially more restrictive than our `SM5_LW10_LOWSPIN_RICH` model, would not be viable for explaining the bulk of our local SMBHs.

Relevant to this point, DCBH formation has long been considered to be possible only under extremely restrictive conditions and therefore only in rare environments, requiring LW fluxes above 1000 J_{21} (Shang et al. 2010; Sugimura et al. 2014; Wolcott-Green et al. 2017). These are much more stringent than any of our DHS models. In fact, in Bhowmick et al. (2022a), we showed that these flux thresholds would produce only a handful of BHs (if any) in our `BRAHMA` volumes. In such a case, lower mass seeds (as in our ESD seed model) would be the only viable origins for the bulk of the local BH populations. However, we are far from having a complete theoretical understanding of the full details of heavy seed formation. In fact, the recent discovery of potentially overmassive BHs by *JWST* (see Section 1) also suggest the possibility that heavy seeds form more frequently than previously thought. Therefore, if we remain agnostic about the formation efficiency of heavy seeds, both low mass and heavy seeds can be viable origins for our local SMBHs. This would make it challenging to ascertain whether our local SMBHs originated from low mass seeds versus heavy seeds (or both).

The above arguments also suggest that better understanding of the formation efficiency of heavy seeds is going to be crucial for determining the origins of local SMBH populations. In order to probe the formation efficiency of heavy seeds, we might have to rely on the observations of $\sim 10^5$ $M_\odot$ BHs at high redshifts ($z \gtrsim 6$), wherein there is a clear distinction in the number density evolution of $\gtrsim 10^5$ $M_\odot$ BHs between the DHS models and the ESD model. In particular, all the DHS models predict much higher number densities than the ESD model at $z \gtrsim 6$ (revisit left panel of Fig. 4). This may have significant consequences on the predicted rates of GW events from merging $\gtrsim 10^5$ $M_\odot$ BHs between low mass versus heavy DCBH seed models at $z \gtrsim 6$. We explore this in ongoing work (Bhowmick et al., in preparation).

4.2 Caveats: uncertainties in modelling of BH accretion, feedback, and dynamics

One of the big challenges in learning about BH seeding from current and future observations, is to navigate potential degeneracies due to uncertainties in the modelling of several other physical processes such as BH accretion and dynamics, star formation, metal enrichment, and stellar and BH feedback. To begin with, since our seed models depend on the formation of dense and metal-poor gas, alternative treatments for star formation and metal enrichment can significantly impact the rates of seed formation at different redshifts. The subsequent growth of these seeds via accretion and mergers can be impacted by the modelling of BH accretion and dynamics. To that end, our work identifies strong sensitivity to seeding in regimes where accretion is suppressed by stellar feedback and the BH growth is dominated by mergers. However, this may be sensitive not just to the choice of the BH accretion model, but also the stellar feedback model.

Notably, when stellar feedback is sufficiently strong, BH accretion may be substantially suppressed regardless of the choice of accretion model. Recent work by Burger et al (in preparation) suggests that this may indeed be the case for the TNG stellar feedback model inherited by our simulations. In such a case, the merger dominated BH growth in low mass galaxies may be fairly robust to the choice of the BH accretion model. However, if the stellar feedback is less strong, the BH growth in low mass galaxies could become much more sensitive to the accretion model. In such a case, the implementation of AGN feedback can also have a profound impact on BH growth. While AGN feedback is well-accepted to be important in massive galaxies, recent observations have also shown evidence for AGN-driven gas outflows in dwarf galaxies (Manzano-King, Canalizo & Sales 2019). In our AGN feedback model adopted from TNG, BH feedback in galaxies from low mass BHs is very weak as the 'kinetic mode' does not switch on until the BH masses are above $\sim 10^8$ $M_\odot$ (and the 'thermal mode' feedback is generally ineffective as most of the deposited thermal energy cools away quickly without much impact). This suggests the need to explore alternative feedback implementations that can allow for the AGN kinetic feedback to operate in galaxies with low mass BHs (for e.g. Koudmani et al. 2024).

Another major source of uncertainty is the modelling of BH dynamics. In this work, by repositioning the BHs, we assume the most optimistic scenario for merger-driven BH growth. In reality, the merging efficiency will depend on the time-scales associated with the hardening of BH binaries due to processes like dynamical friction, stellar scattering, viscous gas drag from circumbinary discs and GW emission. Simulations that use subgrid dynamical friction instead of repositioning (Tremmel et al. 2017; Bellovary et al. 2019; Ni et al. 2022), find a substantial population of BHs that wander away from the local potential minima. Indeed, there is observational evidence of the presence of off-nuclear BHs in local dwarf galaxies (Reines et al. 2020). This is overall important because if a substantial number of BHs wander far enough away from their original host galaxies, it will reduce the overall BH occupation fractions. Gravitational recoil can also lead to BHs getting kicked out of their hosts, further reducing the occupation fractions (Volonteri, Gültekin & Dotti 2010; Blecha et al. 2016; Dunn, Holley-Bockelmann & Bellovary 2020). Since we artificially suppress the possibility of BH wandering, we can interpret

our predicted occupations fractions as upper limits for a given seed model.

In the context of this work, the overall takeaway is the following: we clearly demonstrate that there is strong sensitivity to BH seeding within the context of the assumptions baked into our simulations in $\lesssim 10^6$ M$_\odot$ local BH populations. However, whether we can disentangle these seeding signatures from signatures of other physics, particularly accretion, feedback, and dynamics modelling, remains to be seen. We shall address this in future work.

5 SUMMARY AND CONCLUSIONS

In this paper, we use the BRAHMA cosmological simulations to investigate the mass range where local BH populations may be most sensitive to BH seeding, and to what extent. Our simulations are [18 Mpc]^3 in volume and seed BHs close to the gas mass resolution, with an initial mass of $M_{\rm seed} = 1.5 \times 10^5$ M$_\odot$. These seeds are formed using an array of prescriptions that encompass a broad range of seeding scenarios for heavy seeds as well as lower mass seeds.

Our first four boxes are the same as in Bhowmick et al. (2024c) wherein the 1.5×10^5 M$_\odot$ BHs are directly formed as heavy seeds. In this paper, we refer to them as 'direct heavy seeds' or DHSs. To seed the DHSs, we incrementally stack several seeding criteria motivated by conditions postulated to be crucial for DCBH formation. In the first box (SM5), we place DHSs in all haloes that contain a minimum amount (5 $M_{\rm seed}$) of dense and metal-poor gas. In the second box (SM5_LW10), we additionally require the dense and metal-poor gas to be illuminated by LW radiation ($> 10\ J_{21}$). In the third box (SM5_LW10_LOWSPIN), we further require the seed forming haloes to have gas spins less than the Toomre instability threshold. Finally, we have a fourth box (SM5_LW10_LOWSPIN_RICH) wherein seed formation is further restricted to haloes in rich environments with at least one neighbouring halo of comparable or higher mass. The last criterion is motivated by the possibility that the neighbouring halo will presumably merge and dynamically heat the seed forming halo to create regions where DCBHs can be born without such strong LW radiation.

In addition to the four boxes that seed DHSs, we have a fifth box (ESD:STOCHASTIC) wherein we use our recently developed stochastic seed model (Bhowmick et al. 2024a) to initialize the 1.5×10^5 M$_\odot$ BHs as descendants of lower mass $\sim 10^3$ M$_\odot$ seeds. Since the initial 1.5×10^5 M$_\odot$ BHs are not meant to be the *true seeds*, they are referred to as 'extrapolated seed descendants' or ESDs. In this model, the ESDs are stochastically placed in galaxies with a broad distribution of masses and preferentially living in rich environments. The seed model was calibrated against the highest resolution simulations from Bhowmick et al. (2024b) that explicitly resolved these $\sim 10^3$ M$_\odot$ seeds and traced their growth.

Having five simulation boxes that differ only in their BH seed models enabled us to systematically study the impact of seeding on local BH and AGN populations, for the first time using cosmological hydrodynamic simulations. Our key findings are as follows:

(i) The relative contribution to BH growth from mergers versus gas accretion is a key factor that determines whether BH populations are sensitive to their initial seeding conditions. In our simulations, in the high-z ($z \gtrsim 5$) Universe, the seeding signatures can persist across all BHs at least up to $\sim 10^8$ M$_\odot$, since the BH growth is merger dominated. However, at $z \sim 0$, they tend to get largely erased for $\gtrsim 10^7$ M$_\odot$ BHs due to accretion-driven BH growth. In this regime, all the seed models approach the observational measurements for the BHMFs and $M_* - M_{\rm bh}$ relations.

(ii) At the lowest mass end of $\sim 10^5 - 10^6$ M$_\odot$ BHs, our seed models have a strong impact on our predictions even in the local Universe. This is for two reasons: (1) There is a substantial population of local $\sim 10^5$ M$_\odot$ BHs that are ungrown relics of seeds forming at high redshifts ($z \sim 5 - 10$); (2) The growth of these BHs from $\sim 10^5$ M$_\odot$ to $\sim 10^6$ M$_\odot$ is primarily driven by mergers instead of gas accretion even at $z \sim 0$. The predicted seed model variations in the number densities of $\gtrsim 10^5$ M$_\odot$ BHs range from $0.02 - 0.4$ Mpc^{-3}. For $\gtrsim 10^6$ M$_\odot$ BHs, it ranges from $0.01 - 0.05$ Mpc^{-3}.

(iii) For the ESD model that represents unresolved $\sim 10^3$ M$_\odot$ seeds, the abundances of $\sim 10^6$ M$_\odot$ BHs and $M_{\rm bh}/M_*$ ratios for $\sim 10^5 - 10^6$ M$_\odot$ BHs, are broadly consistent with available observational measurements. This supports $\sim 10^3$ seeds (resembling NSC seeds or extremely massive Pop III seeds) as viable origins for local SMBH populations.

(iv) Amongst the DHS models, the most optimistic SM5 model tends to mildly overpredict the abundances of $\sim 10^6$ M$_\odot$ BHs and $M_{\rm bh}/M_*$ ratios for $\sim 10^5 - 10^6$ M$_\odot$ BHs compared to current observations. The SM5_LW10 and SM5_LW10_LOWSPIN models that additionally include the LW flux criterion and the gas spin criteria, are broadly consistent with both of these observed quantities. The predictions for the most restrictive SM5_LW10_LOWSPIN_RICH seed model are at the lower end of the observational measurements. Overall, these results imply that the heavy DCBH seed models can be viable origins for the local SMBH populations if their formation efficiencies are similar to what is implicitly assumed by our DHS models. Notably, these DHS models are much more plausible origins for local SMBHs compared to several previously proposed DCBH formation scenarios that require much higher LW fluxes ($\gtrsim 1000\ J_{21}$).

(v) The predicted occupation fractions of $\gtrsim 10^5$ M$_\odot$ and $\gtrsim 10^6$ M$_\odot$ BHs in $M_* \sim 10^9$ M$_\odot$ galaxies range from $\sim 40 - 100$ per cent and $\sim 20 - 100$ per cent, respectively, in our simulations. However, the current observational constraints have uncertainties too large to place strong constraints on our seed models.

(vi) We find that the local Universe is more promising than the high-z Universe ($z \sim 5 - 10$) for constraining seed models using AGN LFs. This is because the AGN LFs are sensitive to seed models only at extremely low luminosities of $L_{2-10\ \rm keV} \sim 10^{39}$ erg s^{-1}. These luminosities may be reachable only in the local Universe with possible upcoming missions such as AXIS. However, these entire populations may be far from our reach in the high redshift Universe ($z \gtrsim 5$), even with the next generation of facilities.

Overall, our results affirm current expectations that in the local Universe, BHs with masses around $\sim 10^5 - 10^6$ M$_\odot$ residing in dwarf galaxies are expected to be most strongly impacted by different seed models. But it may still be challenging to ascertain whether the bulk of observed SMBH populations started as low mass seeds, or heavy seeds that form more efficiently than canonical DCBH scenarios. GW events from high-z mergers of $\gtrsim 10^5$ M$_\odot$ BHs may be able to break this degeneracy as it may be a promising probe for the efficiency of heavy seed formation. Deeper EM observations with *JWST* in the future, probing BH to even earlier epochs, may also yield useful constraints. However, signatures of BH accretion, feedback, and dynamics may also be degenerate with BH seeding. For example, here we assume a BH repositioning scheme which promptly merges BH pairs when their host galaxies merge, along with Bondi accretion which leads to slower growth of low mass BHs. Alternative treatments for BH accretion and dynamics could change the relative contribution for mergers versus accretion to BH growth, which can then impact the persistence of seeding signatures. We shall

explore all this in future work. Overall, despite all these caveats, our results do strongly suggest that continued searches for local BHs between $\sim 10^5 - 10^6$ $M_\odot$ can provide strong constraints for BH seeding that would be complementary to the high-z observations from *JWST* and future GW observations of merging BH binaries with LISA.

ACKNOWLEDGEMENTS

This research was supported in part by grant NSFPHY-2309135 to the Kavli Institute for Theoretical Physics (KITP). AKB also acknowledges the organizers of the KITP workshop 'Cosmic Origins: The First Billion Years', during which some of this research was developed. LB acknowledges support from NSF awards AST-1909933 and AST-2307171 and Cottrell Scholar Award #27553 from the Research Corporation for Science Advancement. PT acknowledges support from NSF-AST 2008490. RW acknowledges funding of a Leibniz Junior Research Group (project number J131/2022). LH acknowledges support by the Simons Collaboration on 'Learning the Universe'.

DATA AVAILABILITY

The underlying data used in this work shall be made available upon reasonable request to the corresponding author.

REFERENCES

Agarwal B., Davis A. J., Khochfar S., Natarajan P., Dunlop J. S., 2013, MNRAS, 432, 3438
Aird J., Coil A. L., Georgakakis A., Nandra K., Barro G., Pérez-González P. G., 2015, MNRAS, 451, 1892
Akins H. B. et al., 2024, preprint (arXiv:2406.10341)
Andika I. T. et al., 2024, A&A, 685, A25
Angus C. R. et al., 2022, Nat. Astron., 6, 1452
Bañados E. et al., 2016, ApJS, 227, 11
Bañados E. et al., 2018, Nature, 553, 473
Baldassare V. F., Reines A. E., Gallo E., Greene J. E., 2015, ApJ, 809, L14
Baldassare V. F., Dickey C., Geha M., Reines A. E., 2020, ApJ, 898, L3
Barausse E., 2012, MNRAS, 423, 2533
Barnes J., Hut P., 1986, Nature, 324, 446
Barret D., Decourchelle A., Fabian A., Guainazzi M., Nandra K., Smith R., den Herder J.-W., 2020, Astron. Nachr., 341, 224
Barth A. J., Ho L. C., Rutledge R. E., Sargent W. L. W., 2004, ApJ, 607, 90
Begelman M. C., Silk J., 2023, MNRAS, 526, L94
Begelman M. C., Volonteri M., Rees M. J., 2006, MNRAS, 370, 289
Bellovary J. M., Cleary C. E., Munshi F., Tremmel M., Christensen C. R., Brooks A., Quinn T. R., 2019, MNRAS, 482, 2913
Bhowmick A. K. et al., 2021, MNRAS, 507, 2012
Bhowmick A. K., Blecha L., Torrey P., Kelley L. Z., Vogelsberger M., Nelson D., Weinberger R., Hernquist L., 2022a, MNRAS, 510, 177
Bhowmick A. K. et al., 2022b, MNRAS, 516, 138
Bhowmick A. K., Blecha L., Torrey P., Weinberger R., Kelley L. Z., Vogelsberger M., Hernquist L., Somerville R. S., 2024a, MNRAS, 529, 3768
Bhowmick A. K. et al., 2024b, MNRAS, 531, 4311
Bhowmick A. K. et al., 2024c, MNRAS, 533, 1907
Birchall K. L., Watson M. G., Aird J., 2020, MNRAS, 492, 2268
Blecha L. et al., 2016, MNRAS, 456, 961
Bogdán Á. et al., 2024, Nat. Astron., 8, 126
Bromm V., Loeb A., 2003, ApJ, 596, 34
Buchner J. et al., 2015, ApJ, 802, 89
Burke C. J., Natarajan P., Baldassare V. F., Geha M., 2025, ApJ, 978, 77
Cao X., 2010, ApJ, 725, 388
Chabrier G., 2003, PASP, 115, 763
Chadayammuri U., Bogdán Á., Ricarte A., Natarajan P., 2023, ApJ, 946, 51
Cho H., Prather B. S., Narayan R., Natarajan P., Su K.-Y., Ricarte A., Chatterjee K., 2023, ApJ, 959, L22
Das A., Schleicher D. R. G., Basu S., Boekholt T. C. N., 2021a, MNRAS, 505, 2186
Das A., Schleicher D. R. G., Leigh N. W. C., Boekholt T. C. N., 2021b, MNRAS, 503, 1051
Davies M. B., Miller M. C., Bellovary J. M., 2011, ApJ, 740, L42
Davis M., Efstathiou G., Frenk C. S., White S. D. M., 1985, ApJ, 292, 371
Dayal P., Rossi E. M., Shiralilou B., Piana O., Choudhury T. R., Volonteri M., 2019, MNRAS, 486, 2336
DeGraf C., Sijacki D., 2020, MNRAS, 491, 4973
Desroches L.-B., Greene J. E., Ho L. C., 2009, ApJ, 698, 1515
Di Matteo T., Khandai N., DeGraf C., Feng Y., Croft R. A. C., Lopez J., Springel V., 2012, ApJ, 745, L29
Dijkstra M., Ferrara A., Mesinger A., 2014, MNRAS, 442, 2036
Dong X.-B., Ho L. C., Yuan W., Wang T.-G., Fan X., Zhou H., Jiang N., 2012, ApJ, 755, 167
Dubois Y., Peirani S., Pichon C., Devriendt J., Gavazzi R., Welker C., Volonteri M., 2016, MNRAS, 463, 3948
Dunn G., Holley-Bockelmann K., Bellovary J., 2020, ApJ, 896, 72
Durodola E., Pacucci F., Hickox R. C., 2024, preprint (arXiv:2406.10329)
Evans A. E., Blecha L., Bhowmick A. K., 2025, MNRAS, 536, 2783
Fan X. et al., 2001, AJ, 122, 2833
Filippenko A. V., Ho L. C., 2003, ApJ, 588, L13
Fryer C. L., Woosley S. E., Heger A., 2001, ApJ, 550, 372
Gallo E., Treu T., Marshall P. J., Woo J.-H., Leipski C., Antonucci R., 2010, ApJ, 714, 25
Gallo E. et al., 2023, The black hole occupation fraction of local dwarf galaxies with AXIS, preprint (arXiv:2311.09161), https://arxiv.org/abs/2311.09161
Greene J. E., 2012, Nat. Commun., 3, 1304
Greene J. E., Ho L. C., 2004, ApJ, 610, 722
Greene J. E., Ho L. C., 2007, ApJ, 670, 92
Greene J. E., Strader J., Ho L. C., 2020, ARA&A, 58, 257
Greene J. E. et al., 2024, ApJ, 964, 39
Häberle M. et al., 2024, Nature, 631, 285
Habouzit M., Volonteri M., Latif M., Dubois Y., Peirani S., 2016, MNRAS, 463, 529
Habouzit M., Pisani A., Goulding A., Dubois Y., Somerville R. S., Greene J. E., 2020, MNRAS, 493, 899
Habouzit M. et al., 2021, MNRAS, 503, 1940
Habouzit M. et al., 2022, MNRAS, 509, 3015
Hahn O., Abel T., 2011, MNRAS, 415, 2101
Haidar H. et al., 2022, MNRAS, 514, 4912
Harikane Y. et al., 2023, ApJ, 959, 39
Jeon J., Bromm V., Liu B., Finkelstein S. L., 2025, ApJ, 979, 127
Jiang L. et al., 2016, ApJ, 833, 222
Katz N., Weinberg D. H., Hernquist L., 1996, ApJS, 105, 19
Kaviraj S. et al., 2017, MNRAS, 467, 4739
Khandai N., Di Matteo T., Croft R., Wilkins S., Feng Y., Tucker E., DeGraf C., Liu M.-S., 2015, MNRAS, 450, 1349
King A., Nealon R., 2021, MNRAS, 502, L1
Kocevski D. D. et al., 2023, ApJ, 954, L4
Kocevski D. D. et al., 2024, preprint (arXiv:2404.03576)
Kokorev V. et al., 2023, ApJ, 957, L7
Kokorev V. et al., 2024, ApJ, 968, 38
Kormendy J., Ho L. C., 2013, ARA&A, 51, 511
Koudmani S., Rennehan D., Somerville R. S., Hayward C. C., Anglés-Alcázar D., Orr M. E., Sands I. S., Wellons S., 2024, preprint (arXiv:2409.02172)
Kroupa P., Subr L., Jerabkova T., Wang L., 2020, MNRAS, 498, 5652
Larson R. L. et al., 2023, ApJ, 953, L29
Lin R. et al., 2024, Sci. China Phys. Mech. Astron., 67, 109811
Lodato G., Natarajan P., 2006, MNRAS, 371, 1813
Lodato G., Natarajan P., 2007, MNRAS, 377, L64
Luo Y., Ardaneh K., Shlosman I., Nagamine K., Wise J. H., Begelman M. C., 2018, MNRAS, 476, 3523
Luo Y., Shlosman I., Nagamine K., Fang T., 2020, MNRAS, 492, 4917

Lupi A., Colpi M., Devecchi B., Galanti G., Volonteri M., 2014, MNRAS, 442, 3616
Madau P., Rees M. J., 2001, ApJ, 551, L27
Maiolino R. et al., 2024, A&A, 691, A145
Manzano-King C. M., Canalizo G., Sales L. V., 2019, ApJ, 884, 54
Marconi A., Risaliti G., Gilli R., Hunt L. K., Maiolino R., Salvati M., 2004, MNRAS, 351, 169
Marinacci F. et al., 2018, MNRAS, 480, 5113
Matsuoka Y. et al., 2018, ApJS, 237, 5
Matsuoka Y. et al., 2019, ApJ, 872, L2
Mayer L., Capelo P. R., Zwick L., Di Matteo T., 2024, ApJ, 961, 76
Merloni A., Heinz S., 2008, MNRAS, 388, 1011
Mezcua M., Civano F., Marchesi S., Suh H., Fabbiano G., Volonteri M., 2018, MNRAS, 478, 2576
Mezcua M., Pacucci F., Suh H., Siudek M., Natarajan P., 2024, ApJ, 966, L30
Miller B. P., Gallo E., Greene J. E., Kelly B. C., Treu T., Woo J.-H., Baldassare V., 2015, ApJ, 799, 98
Molina M., Reines A. E., Latimer L. J., Baldassare V., Salehirad S., 2021, ApJ, 922, 155
Mortlock D. J. et al., 2011, Nature, 474, 616
Naiman J. P. et al., 2018, MNRAS, 477, 1206
Natarajan P., 2021, MNRAS, 501, 1413
Natarajan P., Pacucci F., Ferrara A., Agarwal B., Ricarte A., Zackrisson E., Cappelluti N., 2017, ApJ, 838, 117
Natarajan P., Pacucci F., Ricarte A., Bogdán Á., Goulding A. D., Cappelluti N., 2024, ApJ, 960, L1
Nelson D. et al., 2018, MNRAS, 475, 624
Nelson D. et al., 2019a, Comput. Astrophys. Cosmol., 6, 2
Nelson D. et al., 2019b, MNRAS, 490, 3234
Nguyen D. D. et al., 2019, ApJ, 872, 104
Ni Y. et al., 2022, MNRAS, 513, 670
Ni Y., Chen N., Zhou Y., Park M., Yang Y., DiMatteo T., Bird S., Croft R., 2024, The Astrid Simulation: Evolution of black holes and galaxies to z = 0.5 and different evolution pathways for galaxy quenching, preprint (arXiv:2409.10666)
Onoue M. et al., 2023, ApJ, 942, L17
Pacucci F., Nguyen B., Carniani S., Maiolino R., Fan X., 2023, ApJ, 957, L3
Pakmor R., Bauer A., Springel V., 2011, MNRAS, 418, 1392
Pakmor R., Pfrommer C., Simpson C. M., Kannan R., Springel V., 2016, MNRAS, 462, 2603
Pillepich A. et al., 2018a, MNRAS, 473, 4077
Pillepich A. et al., 2018b, MNRAS, 475, 648
Planck Collaboration XIII, 2016, A&A, 594, A13
Prole L. R., Regan J. A., Whalen D. J., Glover S. C. O., Klessen R. S., 2024, A&A, 692, A213
Reed S. L. et al., 2017, MNRAS, 468, 4702
Regan J., Volonteri M., 2024, The Open Journal of Astrophysics, 7, 72
Regan J. A., Haiman Z., Wise J. H., O'Shea B. W., Norman M. L., 2020a, Open J. Astrophys., 3, E9
Regan J. A., Wise J. H., Woods T. E., Downes T. P., O'Shea B. W., Norman M. L., 2020b, Open J. Astrophys., 3, 15
Regan J. A., Wise J. H., O'Shea B. W., Norman M. L., 2020c, MNRAS, 492, 3021
Reines A. E., 2022, Nat. Astron., 6, 26
Reines A. E., Volonteri M., 2015, ApJ, 813, 82
Reines A. E., Greene J. E., Geha M., 2013, ApJ, 775, 116
Reines A. E., Condon J. J., Darling J., Greene J. E., 2020, ApJ, 888, 36
Reynolds C. S. et al., 2023, in Siegmund O. H., Hoadley K., eds, Proc. SPIE Conf. Ser. Vol. 12678, UV, X-Ray, and Gamma-Ray Space Instrumentation for Astronomy XXIII. SPIE, Bellingham, p. 126781E
Ricarte A., Natarajan P., 2018, MNRAS, 481, 3278
Sassano F., Schneider R., Valiante R., Inayoshi K., Chon S., Omukai K., Mayer L., Capelo P. R., 2021, MNRAS, 506, 613
Schaye J. et al., 2015, MNRAS, 446, 521
Schutte Z., Reines A. E., Greene J. E., 2019, ApJ, 887, 245
Shang C., Bryan G. L., Haiman Z., 2010, MNRAS, 402, 1249
Shankar F., Weinberg D. H., Miralda-Escudé J., 2009, ApJ, 690, 20
Shen X., Hopkins P. F., Faucher-Giguère C.-A., Alexander D. M., Richards G. T., Ross N. P., Hickox R. C., 2020, MNRAS, 495, 3252
Sijacki D., Vogelsberger M., Genel S., Springel V., Torrey P., Snyder G. F., Nelson D., Hernquist L., 2015, MNRAS, 452, 575
Smith B., Sigurdsson S., Abel T., 2008, MNRAS, 385, 1443
Smith B. D., Regan J. A., Downes T. P., Norman M. L., O'Shea B. W., Wise J. H., 2018, MNRAS, 480, 3762
Spinoso D., Bonoli S., Valiante R., Schneider R., Izquierdo-Villalba D., 2023, MNRAS, 518, 4672
Springel V., 2010, MNRAS, 401, 791
Springel V., Hernquist L., 2003, MNRAS, 339, 289
Springel V., White S. D. M., Tormen G., Kauffmann G., 2001, MNRAS, 328, 726
Springel V. et al., 2018, MNRAS, 475, 676
Sugimura K., Omukai K., Inoue A. K., 2014, MNRAS, 445, 544
Taylor A. J. et al., 2024, preprint (arXiv:2409.06772)
Terrazas B. A. et al., 2020, MNRAS, 493, 1888
Torrey P., Vogelsberger M., Genel S., Sijacki D., Springel V., Hernquist L., 2014, MNRAS, 438, 1985
Tremmel M., Karcher M., Governato F., Volonteri M., Quinn T. R., Pontzen A., Anderson L., Bellovary J., 2017, MNRAS, 470, 1121
Tremmel M., Ricarte A., Natarajan P., Bellovary J., Sharma R., Quinn T. R., 2024, Open J. Astrophys., 7, 26
Trinca A., Schneider R., Valiante R., Graziani L., Zappacosta L., Shankar F., 2022, MNRAS, 511, 616
Trinca A., Schneider R., Maiolino R., Valiante R., Graziani L., Volonteri M., 2023, MNRAS, 519, 4753
Trinca A. et al., 2024, Episodic super-Eddington accretion as a clue to Over-massive Black Holes in the early Universe, preprint (arXiv:2412.14248)
Venemans B. P. et al., 2015, MNRAS, 453, 2259
Vogelsberger M., Genel S., Sijacki D., Torrey P., Springel V., Hernquist L., 2013, MNRAS, 436, 3031
Vogelsberger M. et al., 2014a, MNRAS, 444, 1518
Vogelsberger M. et al., 2014b, Nature, 509, 177
Vogelsberger M., Marinacci F., Torrey P., Puchwein E., 2020a, Nat. Rev. Phys., 2, 42
Vogelsberger M. et al., 2020b, MNRAS, 492, 5167
Volonteri M., Gültekin K., Dotti M., 2010, MNRAS, 404, 2143
Volonteri M., Dubois Y., Pichon C., Devriendt J., 2016, MNRAS, 460, 2979
Volonteri M. et al., 2020, MNRAS, 498, 2219
Wang F. et al., 2018, ApJ, 869, L9
Wang F. et al., 2021, ApJ, 907, L1
Ward C. et al., 2022, ApJ, 936, 104
Weinberger R. et al., 2017, MNRAS, 465, 3291
Weinberger R. et al., 2018, MNRAS, 479, 4056
Weinberger R., Springel V., Pakmor R., 2020, ApJS, 248, 32
Willott C. J. et al., 2010, AJ, 139, 906
Wise J. H., Regan J. A., O'Shea B. W., Norman M. L., Downes T. P., Xu H., 2019, Nature, 566, 85
Wolcott-Green J., Haiman Z., Bryan G. L., 2017, MNRAS, 469, 3329
Xu H., Wise J. H., Norman M. L., 2013, ApJ, 773, 83
Yang J. et al., 2019, AJ, 157, 236
Yang X., Mohan P., Yang J., Ho L. C., Aditya J. N. H. S., Zhang S., Jaiswal S., Yang X., 2022, ApJ, 941, 43
Zuo W. et al., 2024, ApJ, 974, 288

This paper has been typeset from a TEX/LATEX file prepared by the author.